Zn^{2+} is Essential for Ca^{2+} Oscillations in Mouse Eggs

Hiroki Akizawa[1], Emily Lopes[1,2], Rafael A. Fissore[1*]

[1]Department of Veterinary and Animal Sciences, University of Massachusetts Amherst, 661 North Pleasant Street, Amherst, Massachusetts, 01003, United States.
[2]Molecular and Cellular Biology Graduate Program, University of Massachusetts, Amherst, Massachusetts, 01003, United States.

Running Tittle: Labile Zn^{2+} and Ca^{2+} release

Key Words: Fertilization, mammals, Ca^{2+}, IP_3R1, oocytes, eggs, sperm, divalent cations, chelators

*Author for correspondence (rfissore@umass.edu)

*Rafael A. Fissore
661 North Pleasant Street
ISB-427A
Department of Veterinary and Animal Science
University of Massachusetts, Amherst, 01003
Phone:413-687-5773
Email: rfissore@umass.edu

Abstract

Changes in the intracellular concentration of free calcium (Ca^{2+}) underpin egg activation and initiation of development in animals and plants. In mammals, the Ca^{2+} release is periodical, known as Ca^{2+} oscillations, and mediated by the type 1 inositol 1,4,5-trisphosphate receptor (IP_3R1). Another divalent cation, zinc (Zn^{2+}), increases exponentially during oocyte maturation and is vital for meiotic transitions, arrests, and polyspermy prevention. It is unknown if these pivotal cations interplay during fertilization. Here, using mouse eggs, we showed that basal concentrations of labile Zn^{2+} are indispensable for sperm-initiated Ca^{2+} oscillations because Zn^{2+}-deficient conditions induced by cell-permeable chelators abrogated Ca^{2+} responses evoked by fertilization and other physiological and pharmacological agonists. We also found that chemically- or genetically generated Zn^{2+}-deficient eggs displayed reduced IP_3R1 sensitivity and diminished ER Ca^{2+} leak despite the stable content of the stores and IP_3R1 mass. Resupplying Zn^{2+} restarted Ca^{2+} oscillations, but excessive Zn^{2+} prevented and terminated them, hindering IP_3R1 responsiveness. The findings suggest that a permissive window of Zn^{2+} concentrations is required for Ca^{2+} responses and IP_3R1 function in eggs, ensuring optimal response to fertilization and egg activation.

Introduction

Vertebrate eggs are arrested at the metaphase stage of the second meiosis (MII) when ovulated because they have an active Cdk1/cyclin B complex and inactive APC/C^{Cdc20} (Heim et al., 2018). Release from MII initiates egg activation, the first hallmark of embryonic development (Ducibella et al., 2002; Schultz and Kopf, 1995). The universal signal of egg activation is an increase in the intracellular concentration of calcium (Ca^{2+}) (Ridgway et al., 1977; Stricker, 1999). Ca^{2+} release causes the inactivation of the APC/C inhibitor Emi2, which enhances cyclin B degradation and induces meiotic exit (Lorca et al., 1993; Shoji et al., 2006; Suzuki et al., 2010a). In mammals, the stereotypical fertilization Ca^{2+} signal, oscillations, consists of transient but periodical Ca^{2+} increases that promote progression into interphase (Deguchi et al., 2000; Miyazaki et al., 1986). The sperm-borne Phospholipase C zeta1 (PLCζ) persistently stimulates the production of inositol 1,4,5-trisphosphate (IP_3) (Matsu-ura et al., 2019; Saunders et al., 2002; Wu et al., 2001) that binds its cognate receptor in the endoplasmic reticulum (ER), IP_3R1 and causes Ca^{2+} release from the egg's main Ca^{2+} reservoir (Wakai et al., 2019). The intake of extracellular Ca^{2+} via plasma membrane channels and transporters ensures the persistence of the oscillations (Miao et al., 2012; Stein et al., 2020; Wakai et al., 2019, 2013).

Before fertilization, maturing oocytes undergo cellular and biochemical modifications (see for review (Ajduk et al., 2008)). The nucleus of immature oocytes, known as the germinal vesicle (GV), undergoes the breakdown of its envelope marking the onset of maturation and setting in motion a series of cellular events that culminate with the release of the first polar body, the correct ploidy for fertilization, and re-arrest at MII (Eppig, 1996). Other organelles are also reorganized, such as cortical granules migrate to the cortex for exocytosis and polyspermy block, mitochondria undergo repositioning, and the cytoplasm's redox state becomes progressively reduced to promote the exchange of the sperm's protamine load (Liu, 2011; Perreault et al., 1988; Wakai et al., 2014). Wide-ranging adaptations also occur in the Ca^{2+} release machinery to produce timely and protracted Ca^{2+} oscillations following sperm entry (Fujiwara et al., 1993; Lawrence et al., 1998), including the increase in the content of the Ca^{2+} stores, ER reorganization with cortical cluster formation, and increased IP_3R1 sensitivity (Lee et al., 2006; Wakai et al., 2012). The total intracellular levels of zinc (Zn^{2+}) also remarkably increase during maturation, amounting to a 50% rise, which is necessary for oocytes to proceed to the telophase I of meiosis and beyond (Kim et al., 2010). Remarkably, after fertilization, Zn^{2+} levels need to decrease, as Emi2 is a Zn^{2+}-associated molecule, and high Zn^2 levels prevent MII exit (Bernhardt et al., 2012; Shoji et al., 2014; Suzuki et al., 2010b). Following the initiation of Ca^{2+} oscillations, approximately 10 to 20% of the Zn^{2+} accrued during maturation is ejected during the Zn^{2+} sparks, a conserved event in vertebrates and invertebrate species (Kim et al., 2011; Que et al., 2019; Tokuhiro and Dean, 2018; Wozniak et al., 2020; Zhang et al., 2016). The use of Zn^{2+} chelators such as N,N,N,N-tetrakis (2-pyridinylmethyl)-1,2-ethylenediamine (TPEN) to create Zn^{2+}-deficient conditions buttressed the importance of Zn^{2+} during meiotic transitions (Kim et al., 2010; Suzuki et al., 2010b). However, whether the analogous dynamics of Ca^{2+} and Zn^{2+} during maturation imply crosstalk and Zn^{2+} levels modulate Ca^{2+} release during fertilization is unknown.

IP_3Rs are the most abundant intracellular Ca^{2+} release channel in non-muscle cells (Berridge, 2016). They form a channel by assembling into tetramers with each subunit of ~270kDa MW (Taylor and Tovey, 2010). Mammalian eggs express the type I IP_3R, the most widespread isoform (Fissore et al., 1999; Parrington et al., 1998). IP_3R1 is essential for egg activation because its inhibition precludes Ca^{2+} oscillations (Miyazaki and Ito, 2006; Miyazaki et al., 1992; Xu et al., 2003). Myriad and occasionally cell-specific factors influence Ca^{2+} release through the IP_3R1 (Taylor and Tovey, 2010). For example, following fertilization, IP_3R1 undergoes ligand-induced degradation caused by the sperm-initiated long-lasting production of IP_3 that effectively reduces the IP_3R1 mass

95 (Brind et al., 2000; Jellerette et al., 2000). Another regulatory mechanism is Ca^{2+}, a
96 universal cofactor, which biphasically regulates IP_3Rs' channel opening (Iino, 1990; Jean
97 and Klee, 1986), congruent with several Ca^{2+} and calmodulin binding sites on the
98 channel's sequence (Sienaert et al., 1997; Sipma et al., 1999). Notably, Zn^{2+} may also
99 participate in IP_3R1 regulation. Recent studies using electron cryomicroscopy (cryoEM),
100 a technique that allows peering into the structure of IP_3R1 with a near-atomic resolution,
101 have revealed that a helical linker (LNK) domain near the C-terminus mediates the
102 coupling between the N- and C-terminal ends necessary for channel opening (Fan et al.,
103 2015). The LNK domain contains a putative Zinc-finger motif proposed to be vital for
104 IP_3R1 function (Fan et al., 2015; Paknejad and Hite, 2018). Therefore, the exponential
105 increase in Zn^{2+} levels in maturing oocytes, besides its essential role in meiosis
106 progression, may optimize the IP_3R1 function, revealing hitherto unknown cooperation
107 between these cations during fertilization.

108 Here, we examined whether crosstalk between Ca^{2+} and Zn^{2+} is required to
109 initiate and sustain Ca^{2+} oscillations and maintain Ca^{2+} store content in MII eggs. We
110 found that Zn^{2+}-deficient conditions inhibited Ca^{2+} release and oscillations without
111 reducing Ca^{2+} stores, IP_3 production, IP_3R1 expression, or altering the viability of eggs or
112 zygotes. We show instead that Zn^{2+} deficiency impaired IP_3R1 function and lessened the
113 receptor's ability to gate Ca^{2+} release out of the ER. Remarkably, resupplying Zn^{2+} re-
114 established the oscillations interrupted by low Zn^{2+}, although persistent increases in
115 intracellular Zn^{2+} were harmful, disrupting the Ca^{2+} responses and preventing egg
116 activation. Together, the results show that besides contributing to oocyte maturation, Zn^{2+}
117 has a central function in Ca^{2+} homeostasis such that optimal Zn^{2+} concentrations ensure
118 IP_3R1 function and the Ca^{2+} oscillations required for initiating embryo development.
119

120 **Results**

121 ***TPEN dose-dependently lowers intracellular Zn^{2+} and inhibits sperm-initiated Ca^{2+}***
122 ***oscillations.***

123 TPEN is a cell-permeable, non-specific chelator with a high affinity for transition
124 metals widely used to study their function in cell physiology (Arslan et al., 1985; Lo et
125 al., 2020). Mouse oocytes and eggs have exceedingly high intracellular concentrations of
126 Zn^{2+} (Kim et al., 2011, 2010), and the TPEN-induced defects in the progression of meiosis
127 have been ascribed to its chelation (Bernhardt et al., 2011; Kim et al., 2010). In support
128 of this view, the Zn^{2+} levels of cells showed acute reduction after TPEN addition, as
129 reported by indicators such as FluoZin-3 (Arslan et al., 1985; Suzuki et al., 2010b).
130 Studies in mouse eggs also showed that the addition of mM concentrations of TPEN

131 disrupted Ca^{2+} oscillations initiated by fertilization or $SrCl_2$ (Lawrence et al., 1998;
132 Suzuki et al., 2010b), but the mechanism(s) and target(s) of the inhibition remained
133 unknown. To gain insight into this phenomenon, we first performed dose-titration studies
134 to determine the effectiveness of TPEN in lowering Zn^{2+} in eggs. The addition of 2.5 mM
135 TPEN protractedly reduced Zn^{2+} levels, whereas 5 and 10 mM TPEN acutely and
136 persistently reduced FluoZin-3 fluorescence (**Fig. 1A)**. These concentrations of TPEN are
137 higher than the reported free Zn^{2+} concentrations in cells, but within range of those of
138 found in typical culture conditions (Lo et al., 2020; Qin et al., 2011). We next determined
139 the concentrations of TPEN required to abrogate fertilization-initiated oscillations.
140 Following intracytoplasmic sperm injection (ICSI), we monitored Ca^{2+} responses while
141 increasing TPEN concentrations. As shown in **Fig. 1B**, 5 and 10 μM TPEN effectively
142 blocked ICSI-induced Ca^{2+} oscillations in over half of the treated cells, and the remaining
143 eggs, after a prolonged interval, resumed lower-frequency rises (**Fig. 1B**-center panels).
144 Finally, 50 μM or greater concentrations of TPEN permanently blocked these oscillations
145 (**Fig. 1B**-right panel). It is noteworthy that at the time of addition, TPEN induces a sharp
146 drop in basal Fura-2 F340/ F380 ratios, consistent with Fura-2's high affinity for Zn^{2+}
147 (Snitsarev et al., 1996).
148 We next used membrane-permeable and -impermeable chelators to assess
149 whether TPEN inhibited Ca^{2+} oscillations by chelating Zn^{2+} from intracellular or
150 extracellular compartments. The addition of the high-affinity but cell-impermeable Zn^{2+}
151 chelators DTPA and EDTA neither terminated nor temporarily interrupted ICSI-induced
152 Ca^{2+} oscillations (**Fig. 1C**). Protractedly, Ca^{2+} oscillations slowed down, possibly because
153 of chelation and lowering of external Ca^{2+} (**Fig. 1C**). Conversely, TPA, a permeable Zn^{2+}
154 chelator, blocked the ICSI-initiated oscillations but required higher concentrations than
155 TPEN (**Fig. 1D**). Collectively, the data suggest that basal levels of labile Zn^{2+} are essential
156 to sustain the fertilization-initiated Ca^{2+} oscillations in eggs.
157 We next evaluated whether TPEN supplementation prevented the completion of
158 meiosis and pronuclear (PN) formation following fertilization (**Fig. 1E and Table 1**). All
159 fertilized eggs promptly extruded second polar bodies regardless of treatment (**Fig. 1E**).
160 TPEN, however, impaired PN formation, and by 4- or 7-hr. post-ICSI, most treated eggs
161 failed to show PNs, unlike controls (**Fig. 1E and Table 1**). Together, these results
162 demonstrate that depletion of Zn^{2+} terminates Ca^{2+} oscillations and delays or prevents
163 events of egg activation, including PN formation.
164
165 ***TPEN is a universal inhibitor of Ca^{2+} oscillations in eggs.***
166 Mammalian eggs initiate Ca^{2+} oscillations in response to numerous stimuli and

167 conditions (Miyazaki and Ito, 2006; Wakai and Fissore, 2013). Fertilization and its release
168 of PLCz stimulate the phosphoinositide pathway leading to the production of IP_3 and Ca^{2+}
169 oscillations (Miyazaki, 1988; Saunders et al., 2002). Neurotransmitters such as
170 acetylcholine (Ach) and other G-protein coupled receptor agonists engage a similar
171 mechanism (Dupont et al., 1996; Kang et al., 2003), although in these cases, IP_3
172 production occurs at the plasma membrane and is short-lived (Kang et al., 2003; Swann
173 and Parrington, 1999). Agonists such as $SrCl_2$ and thimerosal generate oscillations by
174 sensitizing IP_3R1 without producing IP_3. The mechanism(s) of $SrCl_2$ is unclear, although
175 its actions are reportedly directly on the IP_3R1 (Hajnóczky and Thomas, 1997; Hamada
176 et al., 2003; Nomikos et al., 2015, 2011; Sanders et al., 2018). Thimerosal oxidizes dozens
177 of thiol groups in the receptor, which enhances the receptor's sensitivity and ability to
178 release Ca^{2+} (Bootman et al., 1992; Evellin et al., 2002; Joseph et al., 2018). We took
179 advantage of the varied points at which the mentioned agonists engage the
180 phosphoinositide pathway to examine TPEN's effectiveness in inhibiting their effects.
181 m*Plcz* mRNA injection, like fertilization, induces persistent Ca^{2+} oscillations, although
182 m*Plcz*'s tends to be more robust. Consistent with this, the addition of 10 and 25 μM TPEN
183 transiently interrupted or belatedly terminated oscillations, whereas 50 μM acutely
184 stopped all responses (**Fig. 2A**). By contrast, $SrCl_2$-initiated rises were the most sensitive
185 to Zn^{2+}-deficient conditions, with 2.5 μM TPEN nearly terminating all oscillations that 5
186 μM did (**Fig. 2B**). TPEN was equally effective in ending the Ach-induced Ca^{2+} responses
187 (**Fig. 2C**), but curbing thimerosal responses required higher concentrations (**Fig. 2D**).
188 Lastly, we ruled out that downregulation of IP_3R1 was responsible for the slow-down or
189 termination of the oscillations by TPEN. To accomplish this, we examined the IP_3R1 mass
190 in eggs (Jellerette et al., 2004) with and without TPEN supplementation and injection of
191 m*Plcz* mRNA. By 4-h post-injection, the mRNA induced the expected down-regulation
192 of IP_3R1 reactivity vs. uninjected eggs, but in TPEN-treated and *Plcz* mRNA-injected
193 eggs, the decrease was insignificant (**Fig. 2F**). These findings together show that Zn^{2+}
194 deficiency inhibits the IP_3R1-mediated Ca^{2+} oscillations independently of IP_3 production
195 or loss of receptor, suggesting a role of Zn^{2+} on IP_3R1 function (**Fig. 2E**).
196
197 ***Zn^{2+} depletion reduces IP_3R1-mediated Ca^{2+} release.***
198 To directly assess the inhibitory effects of TPEN on IP_3R1 function, we used caged
199 IP_3 (cIP_3) that, after short UV pulses, releases IP_3 into the ooplasm (Wakai et al., 2012;
200 Walker et al., 1987). To exclude the possible contribution of external Ca^{2+} to the responses,
201 we performed the experiments in Ca^{2+}-free media. In response to sequential cIP_3 release
202 5 min. apart, control eggs displayed corresponding Ca^{2+} rises that occasionally

203 transitioned into short-lived oscillations (**Fig. 3A**). The addition of TPEN after the third
204 cIP_3 release prevented the subsequent Ca^{2+} response and prematurely terminated the in-
205 progress Ca^{2+} rises (**Fig. 3B and inset)**. Pre-incubation of eggs with TPEN precluded
206 cIP_3-induced Ca^{2+} release, even after 5 sec. of UV exposure (**Fig. 3C**). The addition of
207 excess $ZnSO_4$ (100 μM) overcame TPEN's inhibitory effects, but only if added before
208 **(Fig. 3E)** and not after the addition of TPEN **(Fig. 3D)**. Similar concentrations of $MgCl_2$
209 or $CaCl_2$ failed to reverse TPEN effects **(Fig. 3F, G)**. Together, the results show that Zn^{2+}
210 is required for IP_3R1-mediated Ca^{2+} release downstream of IP_3 production, appearing to
211 interfere with receptor gating, as suggested by TPEN's rapid termination of in-progress
212 Ca^{2+} rises and ongoing oscillations.
213 ERp44 is an ER luminal protein of the thioredoxin family that interacts with the
214 IP_3R1, reportedly inhibiting its ability to mediate Ca^{2+} release (Higo et al., 2005). The
215 localization of ERp44 in the ER-Golgi intermediate compartment of somatic cells
216 correlates with Zn^{2+}'s availability and changes dramatically after TPEN treatment (Higo
217 et al., 2005; Watanabe et al., 2019). To rule out the possibility that TPEN suppresses the
218 function of IP_3R1 by modifying the subcellular distribution of ERp44, we overexpressed
219 ERp44 by injecting HA tagged-*Erp44* mRNA into MII eggs and monitored the effect on
220 Ca^{2+} release. TPEN did not alter the localization of ERp44 (**Supplementary Fig. 1A**),
221 and overexpression of ERp44 modified neither the Ca^{2+} oscillations induced by agonists
222 (**Supplementary Fig. 1B**) nor the effectiveness of TPEN to block them (data not shown).
223 Thus, TPEN and Zn^{2+} deficiency most likely inhibits Ca^{2+} release by directly interfering
224 with IP_3R1 function rather than modifying this particular regulator.
225
226 ***Zn^{2+} depletion diminishes the ER Ca^{2+} leak and increases Ca^{2+} store content.***
227 Our above cIP_3 results that TPEN inhibited IP_3R1-mediated Ca^{2+} release and
228 interrupted in-progress Ca^{2+} rises despite the presence of high levels of environmental IP_3
229 suggest its actions are probably independent of IP_3 binding, agreeing with an earlier report
230 showing that TPEN did not modify IP_3's affinity for the IP_3R (Richardson and Taylor,
231 1993). Additionally, the presence of a Zn^{2+}-binding motif near the C-term cytoplasmic
232 domain of the IP_3R1's channel, which is known to influence agonist-induced IP_3R1 gating
233 (Fan et al., 2015), led us to posit and examine that Zn^{2+} deficiency may be disturbing Ca^{2+}
234 release to the cytosol and out of the ER. To probe this possibility, we queried if pre-
235 treatment with TPEN inhibited Ca^{2+} release through IP_3R1. We first used Thapsigargin
236 (Tg), a Sarcoplasmic/ER Ca^{2+} ATPase pump inhibitor (Thastrup et al., 1990) that unmasks
237 a constitutive Ca^{2+} leak out of the ER (Lemos et al., 2021); in eggs, we have demonstrated
238 it is mediated at least in part by IP_3R1 (Wakai et al., 2019). Treatment with TPEN for 15

239 min. slowed the Tg-induced Ca^{2+} leak into the cytosol, resulting in delayed and lowered
240 amplitude Ca^{2+} responses (**Fig. 4A;** $P<0.05$). To test whether the reduced response to Tg
241 means that TPEN left a temporarily increased Ca^{2+} content in the ER after it, we added
242 the Ca^{2+} ionophore ionomycin (Io), which empties all stores independently of IP_3Rs. Io-
243 induced Ca^{2+} responses were 3.3-fold greater in TPEN-treated cells, supporting the view
244 that TPEN interferes with the ER Ca^{2+} leak **(Fig. 4A;** $P < 0.05$). We further evaluated this
245 concept using *in vitro* aged eggs that often display reduced Ca^{2+} store content than freshly
246 collected counterparts (Abbott et al., 1998). After culturing eggs in the presence or
247 absence of TPEN for 2-hr., we added Io during Ca^{2+} monitoring, which in TPEN-treated
248 eggs induced bigger Ca^{2+} rises than in control eggs **(Fig. 4B;** $P <0.05$**)**. We confirmed that
249 this effect was independent of IP_3R1 degradation because TPEN did not change IP_3R1
250 reactivity in unfertilized eggs (**Fig. 4C**; $P <0.05$).
251 Next, we used the genetically encoded FRET sensor D1ER (Palmer et al., 2004) to
252 assess the TPEN's effect on the ER's relative Ca^{2+} levels changes following the additions
253 of Tg or Ach. TPEN was added 10 min. before 10 μM Tg or 50 μM Ach, and we
254 simultaneously monitored changes in cytosolic and intra-ER Ca^{2+} (**Fig. 4D, E**). For the
255 first three min., the Tg-induced decrease in Ca^{2+}-ER was similar between groups.
256 However, while the drop in Ca^{2+} content continued in control eggs, in TPEN-treated eggs,
257 it came to an abrupt halt, generating profound differences between the two groups (**Fig.
258 4D;** $P <0.05$). TPEN had even more pronounced effects following the addition of Ach,
259 leading to a reduced- and prematurely terminated- Ca^{2+} release from the ER in treated
260 eggs (**Fig. 4E;** $P <0.05$).
261 Lastly, we sought a cellular model where low labile Zn^{2+} occurred without
262 pharmacology. To this end, we examined a genetic model where the two non-selective
263 plasma membrane channels that could influx Zn^{2+} in maturing oocytes have been deleted
264 (Bernhardt et al., 2017; Carvacho et al., 2016, 2013), namely, the transient receptor
265 potential melastatin-7 (TRPM7) and TRP vanilloid 3 (TRPV3), both members of the TRP
266 superfamily of channels (Wu et al., 2010). We found that eggs from double knockout
267 females (dKOs) had lower labile Zn^{2+} levels (**Fig. 4F**), and the addition of Tg revealed an
268 expanded Ca^{2+} store content in these eggs vs. control WT eggs (**Fig. 4G**). Remarkably, in
269 dKO eggs, the Ca^{2+} rise induced by Tg showed a shoulder or inflection point before the
270 peak delaying the time to peak (**Fig. 4G**, **inset**; $P <0.001$). These results in dKO eggs
271 show a changed dynamic of the Tg-induced Ca^{2+} release, suggesting that Zn^{2+} deficient
272 levels modify ER Ca^{2+} release independently of chelators.
273
274 ***Ca^{2+} oscillations in eggs occur within a window of Zn^{2+} concentrations.***

275 We next examined if resupplying Zn^{2+} could restart the Ca^{2+} oscillations
276 terminated by Zn^{2+} depletion. Zn pyrithione (ZnPT) rapidly increases cellular Zn^{2+} upon
277 extracellular addition (Barnett et al., 1977; Robinson, 1964). Dose titration studies and
278 imaging fluorimetry revealed that 0.01 μM ZnPT caused subtle and protracted increases
279 in Zn^{2+} levels, whereas 0.1 μM ZnPT caused rapid increases in eggs' Zn^{2+} baseline (**Fig.**
280 **5A**). We induced detectable Ca^{2+} oscillations by injection of m*Plcz* mRNA followed by
281 50 μM TPEN (**Fig. 5B**), which terminated them. After 30 min, we added 0.1 μM ZnPT,
282 and within 15 min. the oscillations restarted in most TPEN-treated eggs (**Fig. 5C**). We
283 repeated this approach using Thimerosal (**Fig. 5D, E**). Adding 0.1 μM ZnPT did not
284 restore the Ca^{2+} oscillations retrained by TPEN, but 0.5 μM ZnPT did so (**Fig. 5E**). These
285 results demonstrate that Zn^{2+} plays a pivotal, enabling role in the generation of Ca^{2+}
286 oscillations in mouse eggs.
287
288 ***Excessive intracellular Zn^{2+} inhibits Ca^{2+} oscillations.***
289 Zn^{2+} is necessary for diverse cellular functions, consistent with numerous amino
290 acids and proteins capable of binding Zn^{2+} within specific and physiological ranges (Pace
291 and Weerapana, 2014). Excessive Zn^{2+}, however, can cause detrimental effects on cells
292 and organisms (Broun et al., 1990; Hara et al., 2022; Sikora and Ouagazzal, 2021).
293 Consistent with the deleterious effects of Zn^{2+}, a previous study showed that high
294 concentrations of ZnPT, ~50 μM, prevented $SrCl_2$-induced egg activation and initiation
295 of development (Bernhardt et al., 2012; Kim et al., 2011). We examined how ZnPT and
296 excessive Zn^{2+} levels influence Ca^{2+} oscillations. Our conditions revealed that pre-
297 incubation or continuous exposure to 0.1 μM or 1.0 μM ZnPT delayed or prevented egg
298 activation induced by m*Plcz* mRNA injection (**Supplementary Fig. 2**). We used these
299 ZnPT concentrations to add it into ongoing oscillations induced by ICSI and monitored
300 the succeeding Ca^{2+} responses. The addition of 0.05 to 10 μM ZnPT caused an immediate
301 elevation of the basal levels of Fura-2 and termination of the Ca^{2+} oscillations (**Fig. 6A-**
302 **D)**. m*Plcz* mRNA-initiated Ca^{2+} responses were also interrupted by adding 0.1 μM ZnPT,
303 whereas untreated eggs continued oscillating (**Fig. 6E, F**). ZnPT also inhibited IP_3R1-
304 mediated Ca^{2+} release triggered by cIP_3, suggesting that excessive Zn^{2+} directly inhibits
305 IP_3R1 function (**Fig. 6G)**.
306 The increased basal ratios of Fura-2 caused by the addition of ZnPT are unlikely
307 to represent changes in basal Ca^{2+} levels because they would have likely caused some
308 cellular responses such as the release of the second polar body, egg fragmentation, or cell
309 death, neither of which happened. It might reflect, instead, Fura-2's ability to report
310 changes in Zn^{2+} levels, which was the case because the addition of TPEN lowered the

311 Fura-2 ratios without restarting the Ca^{2+} oscillations (**Fig. 6F**). To ensure the impact of
312 ZnPT abolishing Ca^{2+} oscillations was not an imaging artifact obscuring ongoing rises,
313 we simultaneously monitored cytoplasmic and ER Ca^{2+} levels with Rhod-2 and D1ER,
314 respectively. This approach allowed synchronously observing opposite Ca^{2+} changes in
315 the two compartments. In uninjected eggs, the fluorescent values remained unchanged,
316 and in m*Plcz* mRNA-injected eggs, the reporters' signals displayed the expected opposite
317 changes (**Fig. 6H, I**). The addition of ZnPT rapidly increased Rhod-2 signals in uninjected
318 and oscillating eggs, unlike D1ER's, suggesting it cannot detect changes in Zn^{2+} levels to
319 this extent despite faithfully reporting Ca^{2+} changes. In oscillating eggs following ZnPT
320 addition, D1ER progressively showed fewer and lower amplitude changes, consistent
321 with the diminishing and eventual termination of the Ca^{2+} oscillations. Noteworthy, the
322 basal fluorescent ratio of D1ER in these eggs remained unchanged after ZnPT, further
323 demonstrating its unresponsiveness to Zn^{2+} changes of this magnitude. We confirmed that
324 both reporters were still in working order, as the addition of Io triggered Ca^{2+} changes
325 detected by both reporters (**Fig. 6H, I**).
326
327 **Discussion**
328 The present study demonstrates that appropriate levels of labile Zn^{2+} are essential
329 for initiating and maintaining IP_3R1-mediated Ca^{2+} oscillations in mouse eggs regardless
330 of the initiating stimuli. Both deficient and excessive Zn^{2+} compromise IP_3R1 sensitivity,
331 diminishing and mostly terminating Ca^{2+} oscillations. The results demonstrate that IP_3R1
332 and Zn^{2+} act in concert to modulate Ca^{2+} signals revealing previously unexplored
333 crosstalk between these ions at fertilization (**Fig. 7**).
334 Zn^{2+} is an essential micronutrient for living organisms (Kaur et al., 2014) and is
335 required for various cellular functions, such as proliferation, transcription, and
336 metabolism (Lo et al., 2020; Maret and Li, 2009; Yamasaki et al., 2007). Studies using
337 Zn^{2+} chelators have uncovered what appears to be a cell-specific, narrow window of Zn^{2+}
338 concentrations needed for cellular proliferation and survival (Carraway and Dobner,
339 2012; Lo et al., 2020). Further, TPEN appeared especially harmful, and in a few cell lines,
340 even low doses provoked oxidative stress, DNA fragmentation, and apoptosis (Mendivil-
341 Perez et al., 2012). We show here that none of the Zn^{2+} chelators, permeable or
342 impermeable, affected cell viability within our experimental observations, confirming
343 findings from previous studies that employed high concentrations of TPEN to interrupt
344 the Ca^{2+} oscillations (Lawrence et al., 1998) or inducing egg activation of mouse eggs
345 (Suzuki et al., 2010b). Our data demonstrating that ~2.5 mM is the threshold
346 concentration of TPEN in eggs that first causes noticeable changes in basal Zn^{2+}, as

347 revealed by FluoZin, is consistent with the ~2 to 5-mM Zn^{2+} concentrations in most
348 culture media without serum supplementation (Lo et al., 2020), and with the ~100 pM
349 basal Zn^{2+} in cells (Qin et al., 2011). Lastly, the effects on Ca^{2+} release observed here with
350 TPEN and other chelators were due to the chelation of Zn^{2+}, as pretreatment with $ZnSO_4$
351 but not with equal or greater concentrations of $MgCl_2$ or $CaCl_2$ rescued the inhibition of
352 the responses, which is consistent with results by others (Kim et al., 2010; Lawrence et
353 al., 1998).

354 To identify how Zn^{2+} deficiency inhibits Ca^{2+} release in eggs, we induced Ca^{2+}
355 oscillations using various stimuli and tested the effectiveness of membrane-permeable
356 and impermeable chelators to abrogate them. Chelation of extracellular Zn^{2+} failed to
357 terminate the Ca^{2+} responses, whereas membrane-permeable chelators did, pointing to
358 intracellular labile Zn^{2+} levels as essential for Ca^{2+} release. All agonists used here were
359 susceptible to inhibition by TPEN, whether their activities depended on IP_3 production or
360 allosterically induced receptor function, although the effective TPEN concentrations
361 varied across stimuli. Some agents, such as m*Plcz* mRNA or thimerosal, required higher
362 concentrations than $SrCl_2$, Ach, or cIP_3. The reason underlying the different agonists'
363 sensitivities to TPEN will require additional research, but the persistence of IP_3
364 production or change in IP_3R1 structure needed to induce channel gating might explain
365 it. However, the universal abrogation of Ca^{2+} oscillations by TPEN supports the view
366 drawn from cryo-EM-derived IP_3R1 models that signaling molecules can allosterically
367 induce channel gating from different starting positions in the channel by mechanically
368 coupling the binding effect to the ion-conducting pore in the C-terminal end of IP_3R (Fan
369 et al., 2015). The cytosolic C-terminal domain of each IP_3R1 subunit is alongside the IP_3-
370 binding domain of another subunit and, therefore, well positioned to sense IP_3 binding
371 and induce channel gating (Fan et al., 2015). Within each subunit, the LNK domain, which
372 contains a Zn^{2+}-finger motif (Fan et al., 2015), connects the opposite domains of the
373 molecule. Although there are no reports regarding the regulation of IP_3R1 sensitivity by
374 Zn^{2+}, such evidence exists for RyRs (Woodier et al., 2015), which also display a conserved
375 Zn^{2+}-finger motif (des Georges et al., 2016). Lastly, mutations of the two Cys or two His
376 residues of this motif, without exception, resulted in inhibition or inactivation of the IP_3R1
377 channel (Bhanumathy et al., 2012; Uchida et al., 2003). These results are consistent with
378 the view that the C-terminal end of IP_3Rs plays a dominant role in channel gating
379 (Bhanumathy et al., 2012; Uchida et al., 2003). We propose that TPEN inhibits Ca^{2+}
380 oscillations in mouse eggs because chelating Zn^{2+} interferes with the function of the LNK
381 domain and its Zn^{2+}-finger motif proposed role on the mechanical coupling induced by
382 agonist binding to the receptor that propagates to the pore-forming region and required to

383 gate the channel's ion-pore (Fan et al., 2022, 2015).

384 In support of this possibility, TPEN-induced Zn^{2+} deficient conditions altered the
385 Ca^{2+}-releasing kinetics in resting eggs or after fertilization. Tg increases intracellular Ca^{2+}
386 by inhibiting the SERCA pump (Thastrup et al., 1990) and preventing the reuptake into
387 the ER of the ebbing Ca^{2+} during the basal leak. Our previous studies showed that the
388 downregulation of IP_3R1 diminishes the leak, suggesting it occurs through IP_3R1 (Wakai
389 and Fissore, 2019). Consistent with this view, TPEN pre-treatment delayed the Ca^{2+}
390 response induced by Tg, implying that Zn^{2+} deficiency hinders Ca^{2+} release through IP_3R1.
391 An expected consequence would be increased Ca^{2+} content in the ER after Tg. Io that
392 mobilizes Ca^{2+} independently of IP_3Rs (Toeplitz et al., 1979) induced enhanced responses
393 in TPEN-treated eggs vs. controls, confirming the accumulation of Ca^{2+}- ER in Zn^{2+}
394 deficient conditions. We demonstrated that this accumulation is due to hindered emptying
395 of the Ca^{2+} ER evoked by agonists in Zn^{2+}-deficient environments resulting in reduced
396 cytosolic Ca^{2+} increases, as IP_3R1 is the pivotal intermediary channel between these
397 compartments. Noteworthy, the initial phase of the Tg-induced Ca^{2+} release out of the ER
398 did not appear modified by TPEN, as if it was mediated by a Zn^{2+}-insensitive Ca^{2+}
399 channel(s)/transporter, contrasting with Ach-induced emptying that was abrogated from
400 the outset. Remarkably, independently of Zn^{2+} chelators, emptying of Ca^{2+} ER was
401 modified in a genetic model of Zn^{2+}-deficient oocytes lacking two TRP channels,
402 confirming the impact of Zn^{2+} on Ca^{2+} release. It is worth noting that TPEN did not reduce
403 but increased the mass of IP_3R1, which might result in the inhibition of Zn^{2+}-dependent
404 ubiquitin ligase Ubc7 by the Zn-deficient conditions (Webster et al., 2003). We cannot
405 rule out that these conditions may undermine other conformational changes required to
406 trigger IP_3R1 degradation, thereby favoring the accumulation of IP_3R1.

407 Despite accruing Zn^{2+} during oocyte maturation, fertilization witnesses a
408 necessary Zn^{2+} release into the external milieu, known as "Zn^{2+} sparks" (Kim et al., 2011;
409 Que et al., 2019, 2015). This release of Zn^{2+} is a conserved event in fertilization across
410 species and is associated with several biological functions, including those related to
411 fending off polyspermy (Kim et al., 2011; Que et al., 2019; Wozniak et al., 2020). The
412 concomitant decrease in Zn^{2+} facilitates the resumption of the cell cycle and exit from the
413 MII stage (Kim et al., 2011). Congruent with this observation, artificial manipulation that
414 maintains high Zn^{2+} levels prevent egg activation (Kim et al., 2011), whereas lowering
415 Zn^{2+} with chelators leads to egg activation without Ca^{2+} mobilization (Suzuki et al.,
416 2010b). As posed by others, these results suggest that meiosis completion and the early
417 stages of fertilization unfold within a narrow window of permissible Zn^{2+} (Kim et al.,
418 2011, 2010). Here, we extend this concept and show that IP_3R1 function and the Ca^{2+}

419 oscillations in mouse eggs require this optimal level of labile Zn^{2+} because the Ca^{2+}
420 responses interrupted by TPEN-induced Zn^{2+}-insufficiency are rescued by restoring Zn^{2+}
421 levels with ZnPT. Furthermore, unopposed increases in Zn^{2+} by exposure to ZnPT
422 abrogated fertilization-initiated Ca^{2+} oscillations and prevented the expected egg
423 activation events. It is unclear how excess Zn^{2+} disturbs the function of IP_3R1.
424 Nevertheless, IP_3R1s have multiple cysteines whose oxidation enhances the receptor
425 sensitivity to IP_3 (Joseph et al., 2018), and it is possible that excessive Zn^{2+} aberrantly
426 modifies them, disturbing IP_3R1 structure and function. These results reveal a close
427 association between the Zn^{2+} levels controlling meiotic transitions and the Ca^{2+} release
428 necessary for egg activation, placing the IP_3R1 at the center of the crosstalk of these two
429 divalent cations.

430 Abrupt Zn^{2+} changes have emerged as critical signals for meiotic and mitotic
431 transitions in oocytes, eggs, embryos, and somatic cells (Kim et al., 2011, 2010; Lo et al.,
432 2020). Fertilization relies on prototypical Ca^{2+} rises and oscillations, and Zn^{2+} sparks are
433 an egg activation event downstream of this Ca^{2+} release, establishing a functional
434 association between these two divalent cations that continues to grow (Kim et al., 2011).
435 Here, we show that, in addition, these cations actively crosstalk during fertilization and
436 that the fertilization-induced Ca^{2+} oscillations rely on optimized IP_3R1 function
437 underpinned by ideal Zn^{2+} levels set during oocyte maturation. Future studies should
438 explore if artificial alteration of Zn^{2+} levels can extend the fertile lifespan of eggs,
439 improve developmental competence, or for developing non-hormonal methods of
440 contraception.

441 **Materials and Methods**

442 **Key resources table**

Reagent type (species) or resource	Designation	Source or reference	Identifiers	Additional information
Genetic reagent (*Mus musculus*)	CD1	Charles River	022	
Genetic reagent (*Mus musculus*)	C57BL/6J	JAX	JAX: 000664	
Genetic reagent (*Mus musculus*)	*Trpm7*-floxed	A generous gift from Dr. Carmen P. Williams (NIEHS) (PMID: 30322909)		C57BL6/J and 129s4/SvJae mixed background
Genetic reagent (*Mus musculus*)	*Gdf9-cre*	JAX	JAX: 011062	
Genetic reagent (*Mus musculus*)	*Trpv3*$^{-/-}$	A generous gift from Dr H. Xu (PMID: 20403327)		C57BL/6J and 129/SvEv mixed background
Biological sample (mouse oocyte)	*Mus musculus*	this paper		Eggs at the metaphase of the second meiosis
Biological sample (mouse sperm)	*Mus musculus*	this paper		Matured sperm from cauda epididymis
Recombinant DNA reagent	pcDNA6-mouse *Plcz1-venus* (plasmid used as a template for mRNA synthesis)	Published in previous Fissore lab paper PMID: 34313315. Mouse *Plcz1*		mouse *Plcz1* mRNA was fused with Venus and

		sequence was a generous gift from Dr. Kiyoko Fukami (PMID:18028898)		inserted in pcDNA6 vector
Recombinant DNA reagent	pcDNA6-CALR-D1ER-KDEL (plasmid used as a template for mRNA synthesis)	Published in previous Fissore lab paper PMID: 24101727. Original D1ER vector was a generous gift from Dr. Roger Y Tsien (PMID: 15585581)		FRET construct D1ER was inserted between ER-targeting sequence of calreticulin and KDEL ER retention signal in pcDNA6 vector
Recombinant DNA reagent	pcDNA6-human *ERp44-HA* (plasmid used as a template for mRNA synthesis)	This paper. Original human ERp44 sequence was a generous gift from Dr. Roberto Sitia (PMID: 11847130)		human *ERp44* mRNA fused with HA in pcDNA6/ Myc-His B vector
Antibody	Monoclonal HA (Mouse monoclonal)	Roche	11581816001	Dilution: 1:200
Antibody	Polyclonal IP_3R1 (Rabbit polyclonal)	(Parys et al., 1995)		Dilution: 1:1000
Antibody	Monoclonal α-tubulin (Mouse monoclonal)	Sigma-Aldrich	T-9026	Dilution: 1:1000
Antibody	Alexa Fluor 488 (goat anti mouse)	Invitrogen	Invitrogen: A32723	Dilution: 1:400
Commercial assay or kit	T7 mMESSAGE mMACHINE Kit	Invitrogen	Invitrogen: AM1344	Used for *in vitro* mRNA synthesis
Commercial assay or kit	Poly(A) Tailing Kit	Invitrogen	Invitrogen: AM1350	Used for poly (A)

				tailing of synthesized mRNA
Chemical compound, drug	Hyaluronidase from bovine testes	Sigma-Aldrich	H3506	
Chemical compound, drug	3-Isobutyl-1-methylxanthine (IBMX)	Sigma-Aldrich	I5879	
Chemical compound, drug	Polyvinylpyrrolidone (PVP) (average molecular weight: 360,000)	Sigma-Aldrich	PVP360	Used for mRNA microinjection and ICSI
Chemical compound, drug	N,N, N′,N′-Tetrakis (2-pyridylmethyl) ethylenediamine (TPEN)	Sigma-Aldrich	P4413	Prepared in DMSO and kept at –20 °C until use
Chemical compound, drug	Zinc Pyrithione (ZnPT)	Sigma-Aldrich	PHR1401	Prepared in DMSO and kept at –20 °C until use
Chemical compound, drug	Strontium chloride hexahydrate ($SrCl_2$)	Sigma-Aldrich	255521	Freshly dissolved in water on the day of experiment
Chemical compound, drug	Calcium chloride dihydrate ($CaCl_2$)	Sigma-Aldrich	C3881	Freshly dissolved in water on the day of experiment
Chemical compound, drug	Magnesium chloride hexahydrate ($MgCl_2$)	Sigma-Aldrich	M2393	Freshly dissolved in water on the day of experiment
Chemical compound,	Zinc sulfate monohydrate ($ZnSO_4$)	Acros Organics	389802500	Freshly dissolved

drug				in water on the day of experiment
Chemical compound, drug	Ethylenediaminetetraacetic acid sodium dihydrate (EDTA)	LabChem	LC137501	Prepared as 0.5M aqueous solution with pH 8.0 adjusted by NaOH
Chemical compound, drug	Diethylenetriaminepentaacetic acid (DTPA)	Sigma-Aldrich	D6518	
Chemical compound, drug	Tris (2-pyridylmethyl) amine (TPA)	Santa Cruz	sc-477037	
Chemical compound, drug	Dimethyl sulphoxide (DMSO)	Sigma-Aldrich	D8418	Used as a solvent
Chemical compound, drug	Acetylcholine chloride	Sigma-Aldrich	A6625	
Chemical compound, drug	Thimerosal	Sigma-Aldrich	T5125	Freshly dissolved in water on the day of experiment and kept on ice until use
Chemical compound, drug	Ionomycin calcium salt	Tocris	1704	Working concentration: 2.5 µM
Chemical compound, drug	Thapsigargin	Calbiochem	#586500	Working concentration: 10 µM
Other	Pluronic F-127 (20% solution in DMSO) (Pluronic acid)	Invitrogen	P3000MP	
Other	Fura-2 AM	Invitrogen	F1221	Used at

				1.25 mM in TL-HEPES containing 0.02% Pluronic acid
Other	FluoZin-3 AM	Invitrogen	F24195	Used at 1.25 mM in TL-HEPES containing 0.02% Pluronic acid
Other	Fluo-4 AM	Invitrogen	F14201	Used at 1.25 mM in TL-HEPES containing 0.02% Pluronic acid
Other	Rhod2-AM	Invitrogen	R1244	Used at 2.2 mM in TL-HEPES containing 0.02% Pluronic acid.
Other	ci-IP3/ PM	Tocris	6210	Dissolved in DMSO and kept at –20 °C. Before use, the stock was diluted with water to make a final concentration of 0.25 mM.
Other	Pme1	New England	R0560S	Used to

		BioLabs	linearize pcDNA6 vectors for mRNA synthesis
Software, algorithm	Prism	GraphPad Software	Version 5.01

N,N,N′,N′-tetrakis (2-pyridinylmethyl)-1,2-ethylenediamine (TPEN) and Zinc pyrithione (ZnPT) were dissolved in dimethyl sulfoxide (DMSO) at 10 mM and stored at -20°C until use. $SrCl_2$, $CaCl_2$, $ZnSO_4$, and $MgCl_2$ were freshly dissolved with double-sterile water at 1M and diluted with the monitoring media just before use. Ethylenediaminetetraacetic acid (EDTA) and diethylenetriaminepentaacetic acid (DTPA) were reconstituted with double-sterile water at 0.5M and 10 mM, respectively, and the pH was adjusted to 8.0. Tris(2-pyridylmethyl) amine (TPA) was diluted in DMSO at 100 mM and stored at -20°C until use. Acetylcholine chloride and Thimerosal were dissolved in double-sterile water at 550 mM and 100 mM, respectively. Acetylcholine was stored at -20°C until use, whereas Thimerosal was made fresh in each experiment.

Mice

The University of Massachusetts Institutional Animal Care and Use Committee (IACUC) approved all animal experiments and protocols. *Trpm7*-floxed (*Trpm7*$^{fl/fl}$) *Gdf9-Cre* and *Trpv3*$^{-/-}$ mice were bred at our facility. *Trpm7*$^{fl/fl}$ mice were crossed with *Trpv3*$^{-/-}$ to generate *Trpm7*$^{fl/fl}$; *Trpv3*$^{-/-}$ mouse line. Female *Trpm7*$^{fl/fl}$; *Trpv3*$^{-/-}$ mice were crossed with *Trpm7*$^{fl/fl}$; *Trpv3*$^{-/-}$; *Gdf9-cre* male to generate females null for *Trpv3* and with oocyte-specific deletion for *Trpm7*. Ear clips from offspring were collected prior to weaning, and confirmation of genotype was performed after most experiments.

Egg Collection

All gamete handling procedures are as previously reported by us (Wakai and Fissore, 2019). MII eggs were collected from the ampulla of 6- to 8-week-old female mice. Females were superovulated via intraperitoneal injections of 5 IU pregnant mare serum gonadotropin (PMSG, Sigma, St. Louis, MO) and 5 IU human chorionic gonadotropin (hCG, sigma) at 48hr. interval. Cumulus-oocyte-complexes (COCs) were obtained 13.5 hr. post-hCG injection by tearing the ampulla using forceps and needles in TL-HEPES medium. COCs were treated with 0.26% (w/v) of hyaluronidase at room temperature (RT) for 5 min to remove cumulus cells.

473

474 **Intracytoplasmic sperm injection (ICSI)**

475 ICSI was performed as previously reported by us (Kurokawa and Fissore, 2003) using
476 described setup and micromanipulators (Narishige, Japan). Sperm from C57BL/6 or CD1
477 male mice (7-12 weeks old) were collected from the cauda epididymis in TL-HEPES
478 medium, washed several times, heads separated from tails by sonication (XL2020; Heat
479 Systems Inc., USA) for 5 s at 4°C. The sperm lysate was washed in TL-HEPES and
480 diluted with 12% polyvinylpyrrolidone (PVP, MW = 360 kDa) to a final PVP
481 concentration of 6%. A piezo micropipette-driving unit was used to deliver the sperm into
482 the ooplasm (Primetech, Ibaraki, Japan); a few piezo-pulses were applied to puncture the
483 eggs' plasma membrane following penetration of the zona pellucida. After ICSI, eggs
484 were either used for Ca^{2+} monitoring or cultured in KSOM to evaluate activation and
485 development at 36.5°C in a humidified atmosphere containing 5% CO_2.

486

487 **Preparation and microinjection of mRNA**

488 pcDNA6-m*Plcζ-mEGFP*, pcDNA6-CALR-D1ER-KDEL, and pcDNA6-*humanERp44-*
489 *HA* were linearized with the restriction enzyme PmeI and *in vitro* transcribed using the
490 T7 mMESSAGE mMACHINE Kit following procedures previously used in our
491 laboratory (Ardestani et al., 2020). A poly(A) tail was added to the *in vitro* synthesized
492 RNA (mRNA) using Tailing Kit followed by quantification and dilution to 0.5 μg/μL in
493 nuclease-free water and stored at -80°C until use. Before microinjection, m*Plcζ*, D1ER,
494 and *ERp44* mRNA were diluted to 0.01, 1.0, and 0.5 μg/μL, respectively, in nuclease-free
495 water, heated at 95°C for 3 min followed by centrifugation at 13400×*g* for 10 min at 4°C.
496 Cytoplasm injection of mRNA was performed under microscopy equipped with
497 micromanipulators (Narishige, Japan). The zona pellucida and the plasma membrane of
498 MII eggs were penetrated by applying small pulses generated by the piezo
499 micromanipulator (Primetech, Ibaraki, Japan). The preparation of the injection pipette
500 was as for ICSI (Kurokawa and Fissore, 2003), but the diameter of the tip was ~1 μm.

501

502 **Ca^{2+} imaging**

503 Before Ca^{2+} imaging, eggs were incubated in TL-HEPES containing 1.25 μM Fura2-AM,
504 1.25 μM FluoZin3-AM, or 2.2 μM Rhod2-AM and 0.02% Pluronic acid for 20 min at
505 room temperature and then washed. The fluorescent probe-loaded eggs were allowed to
506 attach to the bottom of the glass dish (Mat-Tek Corp., Ashland, MA). Eggs were
507 monitored simultaneously using an inverted microscope (Nikon, Melville, NY) outfitted
508 for fluorescence measurements. Fura-2 AM, FluoZin3-AM, and Rhod2-AM fluorescence

were excited with 340 nm and 380 nm, 480 nm, and 550 nm wavelengths, respectively, every 20 sec, for different intervals according to the experimental design and as previously performed in the laboratory. The illumination was provided by a 75-W Xenon arc lamp and controlled by a filter wheel (Ludl Electronic Products Ltd., Hawthorne, NY). The emitted light above 510 nm was collected by a cooled Photometrics SenSys CCD camera (Roper Scientific, Tucson, AZ). Nikon Element software coordinated the filter wheel and data acquisition. The acquired data were saved and analyzed using Microsoft Excel and GraphPad using Prism software (Ardestani et al., 2020). For Figures 1A, 4A-C, 5A, and 6H-I, values obtained from FluoZin3-AM, Fura2-AM, or Rhod2-AM recordings were divided by the average of the first five recordings for each treatment that was used as the F_0.

To estimate relative changes in Ca^{2+}-ER, emission ratio imaging of the D1ER (YFP/CFP) was performed using a CFP excitation filter, dichroic beamsplitter, CFP and YFP emission filters (Chroma technology, Rockingham, VT; ET436/20X, 89007bs, ET480/40m, and ET535/30m). To measure Ca^{2+}-ER and cytosolic Ca^{2+} simultaneously, eggs that had been injected with D1ER were loaded with Rhod-2AM, and CFP, YFP, and Rhod-2 intensities were collected every 20 seconds.

Caged IP_3

Caged-IP_3/PM (cIP_3) was reconstituted in DMSO and stored at -20°C until use. Before injection, cIP_3 stock was diluted to 0.25 mM with water and microinjected as above. After incubation in KSOM media at 37°C for 1-hr., the injected eggs were loaded with the fluorophore, 1.25 µM Fluo4-AM, and 0.02% Pluronic acid and handled as above for Fura-2 AM. The release of cIP_3 was accomplished by photolysis using 0.5 to 5-sec pulses at 360 nm wavelengths. Ca^{2+} imaging was as above, but Fluo4 was excited at 488 nm wavelength and emitted light above 510 nm collected as above.

Western blot analysis

Cell lysates from 20-50 mouse eggs were prepared by adding 2X- Laemmli sample buffer. Proteins were separated on 5% SDS-PAGE gels and transferred to PVDF membranes (Millipore, Bedford, MA). After blocking with 5% fat-free milk + TBS, membranes were probed with the rabbit polyclonal antibody specific to IP_3R1 (1:1000; a generous gift from Dr. Jan Parys, Katholieke Universiteit, Leuven, Belgium; Parys et al., 1995). Goat anti-rabbit antibody conjugated to horseradish peroxidase (HRP) was used as a secondary antibody (1:5000; Goat anti-Rabbit IgG (H+L) Cross-Adsorbed Secondary Antibody, HRP; Invitrogen, Waltham, Ma). For detection of chemiluminescence, membranes were

545 developed using ECL Prime (Sigma) and exposed for 1–3 min to maximum sensitivity
546 film (VWR, Radnor, PA). Broad-range pre-stained SDS–PAGE molecular weight
547 markers (Bio-Rad, Hercules, CA) were run in parallel to estimate the molecular weight
548 of the immunoreactive bands. The same membranes were stripped at 50°C for 30 min
549 (62.5 mM Tris, 2% SDS, and 100 mM 2-beta mercaptoethanol) and re-probed with anti-
550 α-tubulin monoclonal antibody (1:1000).
551
552 **Immunostaining and confocal microscopy**
553 Immunostaining was performed according to our previous study (Akizawa et al., 2021).
554 After incubation with or without TPEN, MII eggs were fixed with 4% (w/v)
555 paraformaldehyde in house-made phosphate-buffered saline (PBS) for 20 min at room
556 temperature and then permeabilized for 60 min with 0.2% (v/v) Triton X-100 in PBS.
557 Next, the eggs were blocked for 45 min with a blocking buffer containing 0.2% (w/v)
558 skim milk, 2% (v/v) fetal bovine serum, 1% (w/v) bovine serum albumin, 0.1% (v/v)
559 TritonX-100, 0.75% (w/v) glycine in PBS. Eggs were incubated overnight at 4°C with
560 mouse anti-HA antibody (1:200) diluted in blocking buffer. Eggs were washed in blocking
561 buffer 3X for 10 min, followed by incubation at room temperature for 30 min with a
562 secondary antibody, Alexa Fluor 488 goat anti-mouse IgG (H + L) (1:400) diluted in
563 blocking buffer. Fluorescence signals were visualized using a laser-scanning confocal
564 microscope (Nikon A1 Resonant Confocal with six-color TIRF) fitted with a 63×, 1.4 NA
565 oil-immersion objective lens.
566
567 **Statistical analysis**
568 Comparisons for statistical significance of experimental values between treatments and
569 experiments were performed in three or more experiments performed on different batches
570 of eggs in most studies. Given the number of eggs needed, WB studies were repeated
571 twice. Prism-GraphPad software was used to perform the statistical comparisons that
572 include unpaired Student's t-tests, Fisher's exact test, and One-way ANOVA followed by
573 Tukey's multiple comparisons, as applicable, and the production of graphs to display the
574 data. All data are presented as mean±s.d. Differences were considered significant at $P <$
575 0.05.
576
577 **Acknowledgments**
578 We thank Ms. Changli He for technical support and Dr. James Chambers for support with
579 confocal microscopy support. We thank all members of the Fissore lab for useful
580 discussions and suggestions. We thank Jan B. Parys, K.U. Leuven, Belgium, for initial

discussions and advice.

Competing interests

The authors declare no competing or financial interests.

Additional information

Funding Sources

Funder	Grant reference number	Author
National Institute of Health	RO1 HD092499	Rafael A. Fissore
National Institute of Food and Agriculture	2021-06893	MG. Gervasi, R.A. Fissore, P.E. Visconti
Japan Society for the Promotion of Science Overseas Research Fellowship	Postdoctoral fellowship	Hiroki Akizawa
The funders had no role in study design, data collection and interpretation, or the decision to submit the work for publication.		

Author contributions

Hiroki Akizawa, Data curation, Formal analysis, Validation, Investigation, Visualization, Writing—original draft, Writing—review and editing; Emily Lopes, Data curation, Formal analysis, Validation; Rafael A Fissore, Conceptualization, Formal analysis, Supervision, Funding acquisition, Methodology, Writing—original draft, Project administration, Writing—review and editing

References

Abbott AL, Xu Z, Kopf GS, Ducibella T, Schultz RM. 1998. In vitro culture retards spontaneous activation of cell cycle progression and cortical granule exocytosis that normally occur in vivo unfertilized mouse eggs. *Biol Reprod* **59**:1515–1521. doi:10.1095/biolreprod59.6.1515

Ajduk A, Małagocki A, Maleszewski M. 2008. Cytoplasmic maturation of mammalian oocytes: Development of a mechanism responsible for sperm-induced Ca2+ oscillations. *Reprod Biol* **8**:3–22. doi:10.1016/S1642-431X(12)60001-1

Akizawa H, Saito S, Kohri N, Furukawa E, Hayashi Y, Bai H, Nagano M, Yanagawa Y, Tsukahara H, Takahashi M, Kagawa S, Kawahara-Miki R, Kobayashi H, Kono T, Kawahara M. 2021. Deciphering two rounds of cell lineage segregations during bovine preimplantation development. *FASEB J* **35**:1–14. doi:10.1096/fj.202002762RR

609 Ardestani G, Mehregan A, Fleig A, Horgen FD, Carvacho I, Fissore RA. 2020. Divalent
610 cation influx and calcium homeostasis in germinal vesicle mouse oocytes. *Cell*
611 *Calcium* **87**:102181. doi:10.1016/j.ceca.2020.102181
612 Arslan P, Di Virgilio F, Beltrame M. 1985. Cytosolic Ca2+ homeostasis in Ehrlich and
613 Yoshida carcinomas. A new, membrane-permeant chelator of heavy metals reveals
614 that these ascites tumor cell lines have normal cytosolic free Ca2+. *J Biol Chem*
615 **260**:2719–2727. doi:10.1016/s0021-9258(18)89421-2
616 Barnett B, Kretshmar H, Hartman F. 1977. Structural Characterization of Bis (jV-
617 oxopyridine-2-thionato) zinc (II). *Inorg Chem* **16**:1834–1838.
618 Bernhardt ML, Kim AM, O'Halloran T V., Woodruff TK. 2011. Zinc requirement during
619 meiosis I-meiosis II transition in mouse oocytes is independent of the MOS-MAPK
620 pathway. *Biol Reprod* **84**:526–536. doi:10.1095/biolreprod.110.086488
621 Bernhardt ML, Kong BY, Kim AM, O'Halloran T V., Woodruff TK. 2012. A Zinc-
622 Dependent Mechanism Regulates Meiotic Progression in Mammalian Oocytes. *Biol*
623 *Reprod* **86**:1–10. doi:10.1095/biolreprod.111.097253
624 Bernhardt ML, Padilla-Banks E, Stein P, Zhang Y, Williams CJ. 2017. Store-operated
625 Ca2+ entry is not required for fertilization-induced Ca2+ signaling in mouse eggs.
626 *Cell Calcium* **65**:63–72. doi:10.1016/j.ceca.2017.02.004
627 Berridge MJ. 2016. The inositol trisphosphate/calcium signaling pathway in health and
628 disease. *Physiol Rev* **96**:1261–1296. doi:10.1152/physrev.00006.2016
629 Bhanumathy C, Da Fonseca PCA, Morris EP, Joseph SK. 2012. Identification of
630 functionally critical residues in the channel domain of inositol trisphosphate
631 receptors. *J Biol Chem* **287**:43674–43684. doi:10.1074/jbc.M112.415786
632 Bootman MD, Taylor CW, Berridge MJ. 1992. The thiol reagent, thimerosal, evokes Ca2+
633 spikes in HeLa cells by sensitizing the inositol 1,4,5-trisphosphate receptor. *J Biol*
634 *Chem* **267**:25113–25119. doi:10.1016/s0021-9258(19)74013-7
635 Brind S, Swann K, Carroll J. 2000. Inositol 1,4,5-trisphosphate receptors are
636 downregulated in mouse oocytes in response to sperm or adenophostin A but not to
637 increases in intracellular Ca2+ or egg activation. *Dev Biol* **223**:251–265.
638 doi:10.1006/dbio.2000.9728
639 Broun ER, Greist A, Tricot G, Hoffman R. 1990. Excessive Zinc Ingestion: A Reversible
640 Cause of Sideroblastic Anemia and Bone Marrow Depression. *JAMA J Am Med*
641 *Assoc* **264**:1441–1443. doi:10.1001/jama.1990.03450110087033
642 Carraway RE, Dobner PR. 2012. Zinc pyrithione induces ERK- and PKC-dependent
643 necrosis distinct from TPEN-induced apoptosis in prostate cancer cells. *Biochim*
644 *Biophys Acta - Mol Cell Res* **1823**:544–557. doi:10.1016/j.bbamcr.2011.09.013

Carvacho I, Ardestani G, Lee HC, McGarvey K, Fissore RA, Lykke-Hartmann K. 2016. TRPM7-like channels are functionally expressed in oocytes and modulate post-fertilization embryo development in mouse. *Sci Rep* **6**:1–12. doi:10.1038/srep34236

Carvacho I, Lee HC, Fissore RA, Clapham DE. 2013. TRPV3 Channels mediate strontium-induced mouse-egg activation. *Cell Rep* **5**:1375–1386. doi:10.1016/j.celrep.2013.11.007

Deguchi R, Shirakawa H, Oda S, Mohri T, Miyazaki S. 2000. Spatiotemporal analysis of Ca2+ waves in relation to the sperm entry site and animal-vegetal axis during Ca2+ oscillations in fertilized mouse eggs. *Dev Biol* **218**:299–313. doi:10.1006/dbio.1999.9573

des Georges A, Clarke OB, Zalk R, Yuan Q, Condon KJ, Grassucci RA, Hendrickson WA, Marks AR, Frank J. 2016. Structural Basis for Gating and Activation of RyR1. *Cell* **167**:145-157.e17. doi:10.1016/j.cell.2016.08.075

Ducibella T, Huneau D, Angelichio E, Xu Z, Schultz RM, Kopf GS, Fissore R, Madoux S, Ozil J-P. 2002. Egg-to-Embryo Transition Is Driven by Differential Responses to Ca2+ Oscillation Number. *Dev Biol* **250**:280–291. doi:10.1006/dbio.2002.0788

Dupont G, McGuinness OM, Johnson MH, Berridge MJ, Borgese F. 1996. Phospholipase C in mouse oocytes: Characterization of β and γ isoforms and their possible involvement in sperm-induced Ca2+ spiking. *Biochem J* **316**:583–591. doi:10.1042/bj3160583

Eppig JJ. 1996. Coordination of nuclear and cytoplasmic oocyte maturation in eutherian mammals. *Reprod Fertil Dev* **8**:485–489. doi:10.1071/RD9960485

Evellin S, Nolte J, Tysack K, Dorp F Vom, Thiel M, Oude Weernink PA, Jakobs KH, Webb EJ, Lomasney JW, Schmidt M. 2002. Stimulation of phospholipase C-ε by the M3 muscarinic acetylcholine receptor mediated by cyclic AMP and the GTPase Rap2B. *J Biol Chem* **277**:16805–16813. doi:10.1074/jbc.M112024200

Fan G, Baker ML, Wang Z, Baker MR, Sinyagovskiy PA, Chiu W, Ludtke SJ, Serysheva II. 2015. Gating machinery of InsP3R channels revealed by electron cryomicroscopy. *Nature* **527**:336–341. doi:10.1038/nature15249

Fan G, Baker MR, Terry LE, Arige V, Chen M, Seryshev AB, Baker ML, Ludtke SJ, Yule DI, Serysheva II. 2022. Conformational motions and ligand-binding underlying gating and regulation in IP3R channel. *Nat Commun* **13**:1–15. doi:10.1038/s41467-022-34574-1

Fissore RA, Longo FJ, Anderson E, Parys JB, Ducibella T. 1999. Differential distribution of inositol trisphosphate receptor isoforms in mouse oocytes. *Biol Reprod* **60**:49–57. doi:10.1095/biolreprod60.1.49

Fujiwara T, Nakada K, Shirakawa H, Shunichi M. 1993. Development of inositol trisphosphate-induced calcium release mechanism during maturation of hamster oocytes. *Dev Biol*.

Hajnóczky G, Thomas AP. 1997. Minimal requirements for calcium oscillations driven by the IP3 receptor. *EMBO J* **16**:3533–3543. doi:10.1093/emboj/16.12.3533

Hamada K, Terauchi A, Mikoshiba K. 2003. Three-dimensional Rearrangements within Inositol 1,4,5-Trisphosphate Receptor by Calcium. *J Biol Chem* **278**:52881–52889. doi:10.1074/jbc.M309743200

Hara T, Yoshigai E, Ohashi T, Fukada T. 2022. Zinc transporters as potential therapeutic targets: An updated review. *J Pharmacol Sci* **148**:221–228. doi:10.1016/j.jphs.2021.11.007

Heim A, Tischer T, Mayer TU. 2018. Calcineurin promotes APC/C activation at meiotic exit by acting on both XErp1 and Cdc20. *EMBO Rep* **19**:1–10. doi:10.15252/embr.201846433

Higo T, Hattori M, Nakamura T, Natsume T, Michikawa T, Mikoshiba K. 2005. Subtype-specific and ER lumenal environment-dependent regulation of inositol 1,4,5-trisphosphate receptor type 1 by ERp44. *Cell* **120**:85–98. doi:10.1016/j.cell.2004.11.048

Iino M. 1990. Biphasic Ca2+ dependence of inositol 1,4,5-trisphosphate-induced Ca release in smooth muscle cells of the guinea pig taenia caeci. *J Gen Physiol* **95**:1103–1122. doi:10.1085/jgp.95.6.1103

Jean T, Klee CB. 1986. Calcium modulation of inositol 1,4,5-trisphosphate-induced calcium release from neuroblastoma x glioma hybrid (NG108-15) microsomes. *J Biol Chem* **261**:16414–16420. doi:10.1016/s0021-9258(18)66582-2

Jellerette T, He CL, Wu H, Parys JB, Fissore RA. 2000. Down-regulation of the Inositol 1,4,5-Triphosphate Receptor in Mouse Eggs Following Fertilization or Parthenogenetic Activation. *Dev Biol* **223**:238–250. doi:10.1006/dbio.2000.9675

Jellerette T, Kurokawa M, Lee B, Malcuit C, Yoon SY, Smyth J, Vermassen E, De Smedt H, Parys JB, Fissore RA. 2004. Cell cycle-coupled [Ca2+]i oscillations in mouse zygotes and function of the inositol 1,4,5-trisphosphate receptor-1. *Dev Biol* **274**:94–109. doi:10.1016/j.ydbio.2004.06.020

Joseph SK, Young MP, Alzayady K, Yule DI, Ali M, Booth DM, Hajnóczky G. 2018. Redox regulation of type-I inositol trisphosphate receptors in intact mammalian cells. *J Biol Chem* **293**:17464–17476. doi:10.1074/jbc.RA118.005624

Kang D, Park JY, Han J, Bae IH, Yoon SY, Kang SS, Choi WS, Hong SG. 2003. Acetylcholine induces Ca2+ oscillations via m3/m4 muscarinic receptors in the

717 mouse oocyte. *Pflugers Arch Eur J Physiol* **447**:321–327. doi:10.1007/s00424-003-
718 1184-y
719 Kaur K, Gupta R, Saraf SA, Saraf SK. 2014. Zinc: The metal of life. *Compr Rev Food*
720 *Sci Food Saf* **13**:358–376. doi:10.1111/1541-4337.12067
721 Kim AM, Bernhardt ML, Kong BY, Ahn RW, Vogt S, Woodruff TK, O'Halloran T V. 2011.
722 Zinc sparks are triggered by fertilization and facilitate cell cycle resumption in
723 mammalian eggs. *ACS Chem Biol* **6**:716–723. doi:10.1021/cb200084y
724 Kim AM, Vogt S, O'Halloran T V., Woodruff TK. 2010. Zinc availability regulates exit
725 from meiosis in maturing mammalian oocytes. *Nat Chem Biol* **6**:674–681.
726 doi:10.1038/nchembio.419
727 Kurokawa M, Fissore RA. 2003. ICSI-generated mouse zygotes exhibit altered calcium
728 oscillations, inositol 1,4,5-trisphosphate receptor-1 down-regulation, and embryo
729 development. *Mol Hum Reprod* **9**:523–533. doi:10.1093/molehr/gag072
730 Lawrence Y, Ozil JP, Swann K. 1998. The effects of a Ca2+ chelator and heavy-metal-ion
731 chelators upon Ca2+ oscillations and activation at fertilization in mouse eggs suggest
732 a role for repetitive Ca2+ increases. *Biochem J* **335**:335–342.
733 doi:10.1042/bj3350335
734 Lee B, Vermassen E, Yoon SY, Vanderheyden V, Ito J, Alfandari D, De Smedt H, Parys
735 JB, Fissore RA. 2006. Phosphorylation of IP3R1 and the regulation of [Ca2+]i
736 responses at fertilization: A role for the MAP kinase pathway. *Development*
737 **133**:4355–4365. doi:10.1242/dev.02624
738 Lemos FO, Bultynck G, Parys JB. 2021. A comprehensive overview of the complex world
739 of the endo- and sarcoplasmic reticulum Ca2+-leak channels. *Biochim Biophys Acta*
740 *- Mol Cell Res* **1868**:119020. doi:10.1016/j.bbamcr.2021.119020
741 Liu M. 2011. The biology and dynamics of mammalian cortical granules. *Reprod Biol*
742 *Endocrinol* **9**:1–17. doi:10.1186/1477-7827-9-149
743 Lo MN, Damon LJ, Tay JW, Jia S, Palmer AE. 2020. Single cell analysis reveals multiple
744 requirements for zinc in the mammalian cell cycle. *Elife* **9**:1–24.
745 doi:10.7554/eLife.51107
746 Lorca T, Cruzalegui FH, Fesquet D, Cavadore J, Méry J, Means A, Marcel D. 1993.
747 Calmodulin-dependent protein kinase II mediates inactivation of MPF and CSF upon
748 fertilization of Xenopus eggs. *Nature* **366**:270–273.
749 Maret W, Li Y. 2009. Coordination dynamics of zinc in proteins. *Chem Rev* **109**:4682–
750 4707. doi:10.1021/cr800556u
751 Matsu-ura T, Shirakawa H, Suzuki KGN, Miyamoto A, Sugiura K, Michikawa T, Kusumi
752 A, Mikoshiba K. 2019. Dual-FRET imaging of IP 3 and Ca 2+ revealed Ca 2+ -

induced IP 3 production maintains long lasting Ca 2+ oscillations in fertilized mouse eggs. *Sci Rep* **9**:1–11. doi:10.1038/s41598-019-40931-w

Mendivil-Perez M, Velez-Pardo C, Jimenez-Del-Rio M. 2012. TPEN induces apoptosis independently of zinc chelator activity in a model of acute lymphoblastic leukemia and Ex vivo acute leukemia cells through oxidative stress and mitochondria caspase-3- and AIF-dependent pathways. *Oxid Med Cell Longev* **2012**. doi:10.1155/2012/313275

Miao YL, Stein P, Jefferson WN, Padilla-Banks E, Williams CJ. 2012. Calcium influx-mediated signaling is required for complete mouse egg activation. *Proc Natl Acad Sci U S A* **109**:4169–4174. doi:10.1073/pnas.1112333109

Miyazaki S. 1988. Inositol 1,4,5-trisphosphate-induced calcium release and guanine nucleotide-binding protein-mediated periodic calcium rises in golden hamster eggs. *J Cell Biol* **106**:345–353.

Miyazaki S, Ito M. 2006. Calcium signals for egg activation in mammals. *J Pharmacol Sci* **100**:545–552. doi:10.1254/jphs.CPJ06003X

Miyazaki SI, Hashimoto N, Yoshimoto Y, Kishimoto T, Igusa Y, Hiramoto Y. 1986. Temporal and spatial dynamics of the periodic increase in intracellular free calcium at fertilization of golden hamster eggs. *Dev Biol* **118**:259–267. doi:10.1016/0012-1606(86)90093-X

Miyazaki SI, Yuzaki M, Nakada K, Shirakawa H, Nakanishi S, Nakade S, Mikoshiba K. 1992. Block of Ca2+ wave and Ca2+ oscillation by antibody to the inositol 1,4,5-trisphosphate receptor in fertilized hamster eggs. *Science (80-)* **257**:251–255. doi:10.1126/science.1321497

Nomikos M, Elgmati K, Theodoridou M, Calver BL, Nounesis G, Swann K, Lai FA. 2011. Phospholipase Cζ binding to PtdIns(4,5)P 2 requires the XY-linker region. *J Cell Sci* **124**:2582–2590. doi:10.1242/jcs.083485

Nomikos M, Sanders JR, Parthimos D, Buntwal L, Calver BL, Stamatiadis P, Smith A, Clue M, Sideratou Z, Swann K, Lai FA. 2015. Essential role of the EF-hand domain in targeting sperm phospholipase Cζ to membrane phosphatidylinositol 4,5-bisphosphate (PIP2). *J Biol Chem* **290**:29519–29530. doi:10.1074/jbc.M115.658443

Pace NJ, Weerapana E. 2014. A competitive chemical-proteomic platform to identify zinc-binding cysteines. *ACS Chem Biol* **9**:258–265. doi:10.1021/cb400622

Paknejad N, Hite RK. 2018. Structural basis for the regulation of inositol trisphosphate receptors by Ca2+ and IP3. *Nat Struct Mol Biol* **25**:660–668. doi:10.1038/s41594-018-0089-6

Palmer AE, Jin C, Reed JC, Tsien RY. 2004. Bcl-2-mediated alterations in endoplasmic

789 reticulum Ca2+ analyzed with an improved genetically encoded fluorescent sensor.
790 *Proc Natl Acad Sci U S A* **101**:17404–17409. doi:10.1073/pnas.0408030101
791 Parrington J, Brind S, De Smedt H, Gangeswaran R, Anthony Lai F, Wojcikiewicz R,
792 Carroll J. 1998. Expression of inositol 1,4,5-trisphosphate receptors in mouse
793 oocytes and early embryos: The type I isoform is upregulated in oocytes and
794 downregulated after fertilization. *Dev Biol* **203**:451–461.
795 doi:10.1006/dbio.1998.9071
796 Parys JB, De Smedt H, Missiaen L, Bootman MD, Sienaert I, Casteels R. 1995. Rat
797 basophiliv leukemia cells as model system for inositol 1,4,5-trisphosphate receptor
798 IV, a receptor of the type II family: functional comparison and immunological
799 detection. *Cell Calcium* **17**:239–249. doi:10.1016/0143-4160(95)90070-5
800 Perreault SD, Barbee RR, Slott VL. 1988. Importance of glutathione in the acquisition
801 and maintenance of sperm nuclear decondensing activity in maturing hamster
802 oocytes. *Dev Biol* **125**:181–186. doi:10.1016/0012-1606(88)90070-X
803 Qin Y, Dittmer PJ, Park JG, Jansen KB, Palmer AE. 2011. Measuring steady-state and
804 dynamic endoplasmic reticulum and Golgi Zn 2+ with genetically encoded sensors.
805 *Proc Natl Acad Sci U S A* **108**:7351–7356. doi:10.1073/pnas.1015686108
806 Que EL, Bleher R, Duncan FE, Kong BY, Gleber SC, Vogt S, Chen S, Garwin SA, Bayer
807 AR, Dravid VP, Woodruff TK, O'Halloran T V. 2015. Quantitative mapping of zinc
808 fluxes in the mammalian egg reveals the origin of fertilization-induced zinc sparks.
809 *Nat Chem* **7**:130–139. doi:10.1038/nchem.2133
810 Que EL, Duncan FE, Lee HC, Hornick JE, Vogt S, Fissore RA, O'Halloran T V., Woodruff
811 TK. 2019. Bovine eggs release zinc in response to parthenogenetic and sperm-
812 induced egg activation. *Theriogenology* **127**:41–48.
813 doi:10.1016/j.theriogenology.2018.12.031
814 Richardson A, Taylor CW. 1993. Effects of Ca2+ chelators on purified inositol 1,4,5-
815 trisphosphate (InsP3) receptors and InsP3-stimulated Ca2+ mobilization. *J Biol*
816 *Chem* **268**:11528–11533. doi:10.1016/s0021-9258(19)50232-0
817 Ridgway EB, Gilkey JC, Jaffe LF. 1977. Free calcium increases explosively in activating
818 medaka eggs. *Proc Natl Acad Sci U S A* **74**:623–627. doi:10.1073/pnas.74.2.623
819 Robinson MA. 1964. Complexes of 1-hydroxy 2-pyridinethione. *J Inorg Nucl Chem*
820 **26**:1277–1281. doi:10.1016/0022-1902(64)80210-4
821 Sanders JR, Ashley B, Moon A, Woolley TE, Swann K. 2018. PLCζ induced Ca2+
822 oscillations in mouse eggs involve a positive feedback cycle of Ca2+ induced InsP3
823 formation from cytoplasmic PIP2. *Front Cell Dev Biol* **6**:1–14.
824 doi:10.3389/fcell.2018.00036

825 Saunders CM, Larman MG, Parrington J, Cox LJ, Royse J, Blayney LM, Swann K, Lai
826 FA. 2002. PLC zeta: a sperm-specific trigger of Ca(2+) oscillations in eggs and
827 embryo development. *Development* **129**:3533–44.
828 Schultz RM, Kopf GS. 1995. Molecular Basis of Mammalian Egg Activation. *Curr Top*
829 *Dev Biol* **30**:21–62. doi:10.1007/978-3-642-83139-3_7
830 Shoji S, Muto Y, Ikeda M, He F, Tsuda K, Ohsawa N, Akasaka R, Terada T, Wakiyama
831 M, Shirouzu M, Yokoyama S. 2014. The zinc-binding region (ZBR) fragment of
832 Emi2 can inhibit APC/C by targeting its association with the coactivator Cdc20 and
833 UBE2C-mediated ubiquitylation. *FEBS Open Bio* **4**:689–703.
834 doi:10.1016/j.fob.2014.06.010
835 Shoji S, Yoshida N, Amanai M, Ohgishi M, Fukui T, Fujimoto S, Nakano Y, Kajikawa E,
836 Perry ACF. 2006. Mammalian Emi2 mediates cytostatic arrest and transduces the
837 signal for meiotic exit via Cdc20. *EMBO J* **25**:834–845.
838 doi:10.1038/sj.emboj.7600953
839 Sienaert I, Missiaen L, De Smedt H, Parys JB, Sipma H, Casteels R. 1997. Molecular and
840 functional evidence for multiple Ca2+-binding domains in the type 1 inositol 1,4,5-
841 trisphosphate receptor. *J Biol Chem* **272**:25899–25906.
842 doi:10.1074/jbc.272.41.25899
843 Sikora J, Ouagazzal AM. 2021. Synaptic zinc: An emerging player in Parkinson's disease.
844 *Int J Mol Sci* **22**:1–16. doi:10.3390/ijms22094724
845 Sipma H, De Smet P, Sienaert I, Vanlingen S, Missiaen L, Parys JB, De Smedt H. 1999.
846 Modulation of inositol 1,4,5-trisphosphate binding to the recombinant ligand-
847 binding site of the type-1 inositol 1,4,5-trisphosphate receptor by Ca2+ and
848 calmodulin. *J Biol Chem* **274**:12157–12162. doi:10.1074/jbc.274.17.12157
849 Snitsarev VA, McNulty TJ, Taylor CW. 1996. Endogenous heavy metal ions perturb fura-
850 2 measurements of basal and hormone-evoked Ca2+ signals. *Biophys J* **71**:1048–
851 1056. doi:10.1016/S0006-3495(96)79305-0
852 Stein P, Savy V, Williams AM, Williams CJ. 2020. Modulators of calcium signalling at
853 fertilization. *Open Biol* **10**. doi:10.1098/rsob.200118
854 Stricker SA. 1999. Comparative biology of calcium signaling during fertilization and egg
855 activation in animals. *Dev Biol* **211**:157–176. doi:10.1006/dbio.1999.9340
856 Suzuki T, Suzuki E, Yoshida N, Kubo A, Li H, Okuda E, Amanai M, Perry ACF. 2010a.
857 Mouse Emi2 as a distinctive regulatory hub in second meiotic metaphase.
858 *Development* **137**:3281–3291. doi:10.1242/dev.052480
859 Suzuki T, Yoshida N, Suzuki E, Okuda E, Perry ACF. 2010b. Full-term mouse
860 development by abolishing Zn2+-dependent metaphase II arrest without Ca2+

release. *Development* **137**:2659–2669. doi:10.1242/dev.049791

Swann K, Parrington J. 1999. Mechanism of Ca2+ release at fertilization in mammals. *J Exp Zool* **285**:267–275. doi:10.1002/(SICI)1097-010X(19991015)285:3<267::AID-JEZ10>3.0.CO;2-P

Taylor CW, Tovey SC. 2010. IP3 Receptors: Toward Understanding Their Activation. *Cold Spring Harb Perspect Biol* **2**:1–23.

Thastrup O, Cullen PJ, Drobak BK, Hanley MR, Dawson AP. 1990. Thapsigargin, a tumor promoter, discharges intracellular Ca2+ stores by specific inhibition of the endoplasmic reticulum Ca2+-ATPase. *Proc Natl Acad Sci U S A* **87**:2466–2470. doi:10.1073/pnas.87.7.2466

Toeplitz BK, Cohen AI, Funke PT, Parker WL, Gougoutas JZ. 1979. Structure of Ionomycin—A Novel Diacidic Polyether Antibiotic Having High Affinity for Calcium Ions. *J Am Chem Soc* **101**:3344–3353. doi:10.1021/ja00506a035

Tokuhiro K, Dean J. 2018. Glycan-Independent Gamete Recognition Triggers Egg Zinc Sparks and ZP2 Cleavage to Prevent Polyspermy. *Dev Cell* **46**:627-640.e5. doi:10.1016/j.devcel.2018.07.020

Uchida K, Miyauchi H, Furuichi T, Michikawa T, Mikoshiba K. 2003. Critical regions for activation gating of the inositol 1,4,5-trisphosphate receptor. *J Biol Chem* **278**:16551–16560. doi:10.1074/jbc.M300646200

Wakai T, Fissore RA. 2019. Constitutive IP3R1-mediated Ca2+ release reduces Ca2+ store content and stimulates mitochondrial metabolism in mouse GV oocytes. *J Cell Sci* **132**. doi:10.1242/jcs.225441

Wakai T, Fissore RA. 2013. Ca2+ homeostasis and regulation of ER Ca2+ in mammalian oocytes/eggs. *Cell Calcium* **53**:63–67. doi:10.1016/j.ceca.2012.11.010

Wakai T, Harada Y, Miyado K, Kono T. 2014. Mitochondrial dynamics controlled by mitofusins define organelle positioning and movement during mouse oocyte maturation. *Mol Hum Reprod* **20**:1090–1100. doi:10.1093/molehr/gau064

Wakai T, Mehregan A, Fissore RA. 2019. Ca2+ signaling and homeostasis in mammalian oocytes and eggs. *Cold Spring Harb Perspect Biol* **11**. doi:10.1101/cshperspect.a035162

Wakai T, Vanderheyden V, Yoon SY, Cheon B, Zhang N, Parys JB, Fissore RA. 2012. Regulation of inositol 1,4,5-trisphosphate receptor function during mouse oocyte maturation. *J Cell Physiol* **227**:705–717. doi:10.1002/jcp.22778

Wakai T, Zhang N, Vangheluwe P, Fissore RA. 2013. Regulation of endoplasmic reticulum Ca2+ oscillations in mammalian eggs. *J Cell Sci* **126**:5714–5724. doi:10.1242/jcs.136549

Walker JW, Somlyo A V., Goldman YE, Somlyo AP, Trentham DR. 1987. Kinetics of smooth and skeletal muscle activation by laser pulse photolysis of caged inositol 1,4,5-trisphosphate. *Nature* **327**:249–252.

Watanabe S, Amagai Y, Sannino S, Tempio T, Anelli T, Harayama M, Masui S, Sorrentino I, Yamada M, Sitia R, Inaba K. 2019. Zinc regulates ERp44-dependent protein quality control in the early secretory pathway. *Nat Commun* **10**:1–16. doi:10.1038/s41467-019-08429-1

Webster JM, Tiwari S, Weissman AM, Wojcikiewicz RJH. 2003. Inositol 1,4,5-trisphosphate receptor ubiquitination is mediated by mammalian Ubc7, a component of the endoplasmic reticulum-associated degradation pathway, and is inhibited by chelation of intracellular Zn2+. *J Biol Chem* **278**:38238–38246. doi:10.1074/jbc.M305600200

Woodier J, Rainbow RD, Stewart AJ, Pitt SJ. 2015. Intracellular zinc modulates cardiac ryanodine receptor-mediated calcium release. *J Biol Chem* **290**:17599–17610. doi:10.1074/jbc.M115.661280

Wozniak KL, Bainbridge RE, Summerville DW, Tembo M, Phelps WA, Sauer ML, Wisner BW, Czekalski ME, Pasumarthy S, Hanson ML, Linderman MB, Luu CH, Boehm ME, Sanders SM, Buckley KM, Bain DJ, Nicotra ML, Lee MT, Carlson AE. 2020. Zinc protection of fertilized eggs is an ancient feature of sexual reproduction in animals. *PLoS Biol* **18**:1–17. doi:10.1371/journal.pbio.3000811

Wu H, Smyth J, Luzzi V, Fukami K, Takenawa T, Black SL, Allbritton NL, Fissore RA. 2001. Sperm factor induces intracellular free calcium oscillations by stimulating the phosphoinositide pathway. *Biol Reprod* **64**:1338–1349. doi:10.1095/biolreprod64.5.1338

Wu L, Sweet T, Clapham DE. 2010. Current Progress in the Mammalian TRP Ion Channel Family. *Pharmocol Rev* **62**:381–404. doi:10.1124/pr.110.002725.Abbreviations

Xu Z, Williams CJ, Kopf GS, Schultz RM. 2003. Maturation-associated increase in IP3 receptor type 1: Role in conferring increased IP3 sensitivity and Ca2+ oscillatory behavior in mouse eggs. *Dev Biol* **254**:163–171. doi:10.1016/S0012-1606(02)00049-0

Yamasaki S, Sakata-Sogawa K, Hasegawa A, Suzuki T, Kabu K, Sato E, Kurosaki T, Yamashita S, Tokunaga M, Nishida K, Hirano T. 2007. Zinc is a novel intracellular second messenger. *J Cell Biol* **177**:637–645. doi:10.1083/jcb.200702081

Zhang N, Duncan FE, Que EL, O'Halloran T V., Woodruff TK. 2016. The fertilization-induced zinc spark is a novel biomarker of mouse embryo quality and early development. *Sci Rep* **6**:1–9. doi:10.1038/srep22772

933

934 **Table**

935 **Table 1. Addition of TPEN after ICSI does not prevent extrusion of the second polar**
936 **body but precludes pronuclear (PN) formation.**

Group*	No. of zygotes	2nd polar body (2.5h)	PN	
			4h	7h
Untreated	26	25 (96.1%)	23 (88.5%)	23 (88.5%)
TPEN (10μM)	27	24 (88.9%)	1 (3.7%)***	2 (7.4%)***

937 ***$P < 0.001$

938 *Data from three different replicates for each group.

939 **Figures and Legends**

940 **Figure 1. TPEN-induced Zn^{2+} deficiency inhibits fertilization-initiated $[Ca^{2+}]_i$ oscillations in a**
941 **dose-dependent manner.**

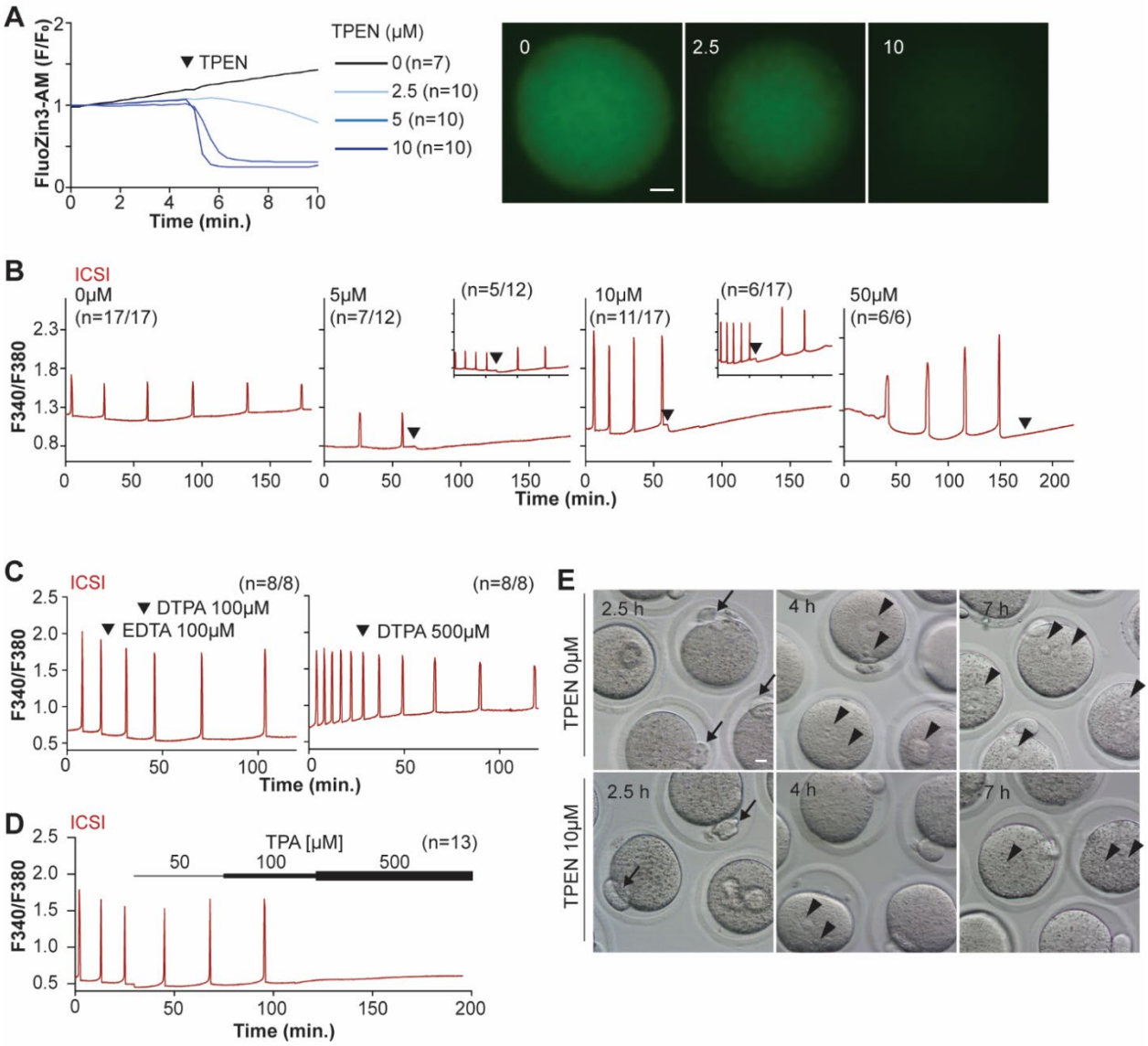

942

943 (**A**) (Left panel) Representative normalized Zn^{2+} recordings of MII eggs loaded with FluoZin-3AM
944 following the addition of increasing concentrations of TPEN (0 μM, DMSO, black trace; 2.5 μM, sky
945 blue; 5 μM, blue; 10 μM, navy). TPEN was directly added to the monitoring media. (Right panel)
946 Representative fluorescent images of MII eggs loaded FluoZin-3AM supplemented with 0, 2.5, and 10
947 μM of TPEN. Scale bar: 10 μm. (**B-D**). (**B**) Representative Ca^{2+} oscillations following ICSI after the
948 addition of 0, 5, 10, or 50 μM TPEN (arrowheads). Insets show representative traces for eggs that
949 resumed Ca^{2+} oscillations after TPEN. (**C**) As above, but following the addition of 100 μM EDTA, 100
950 or 500 μM DTPA (time of addition denoted by arrowheads). (**D**) Ca^{2+} oscillations following ICSI after
951 the addition of 50, 100, and 500 μM TPA (horizontal bars of increasing thickness). (**E**) Representative
952 bright field images of ICSI fertilized eggs 2.5, 4, and 7 hr. after sperm injection. Arrows and
953 arrowheads denote the second polar body and PN formation, respectively. Scale bar: 10 μm.

Figure 2. TPEN dose-dependently inhibits Ca^{2+} oscillations in eggs triggered by a broad-spectrum of agonists that stimulate the PI pathway or IP_3R1.

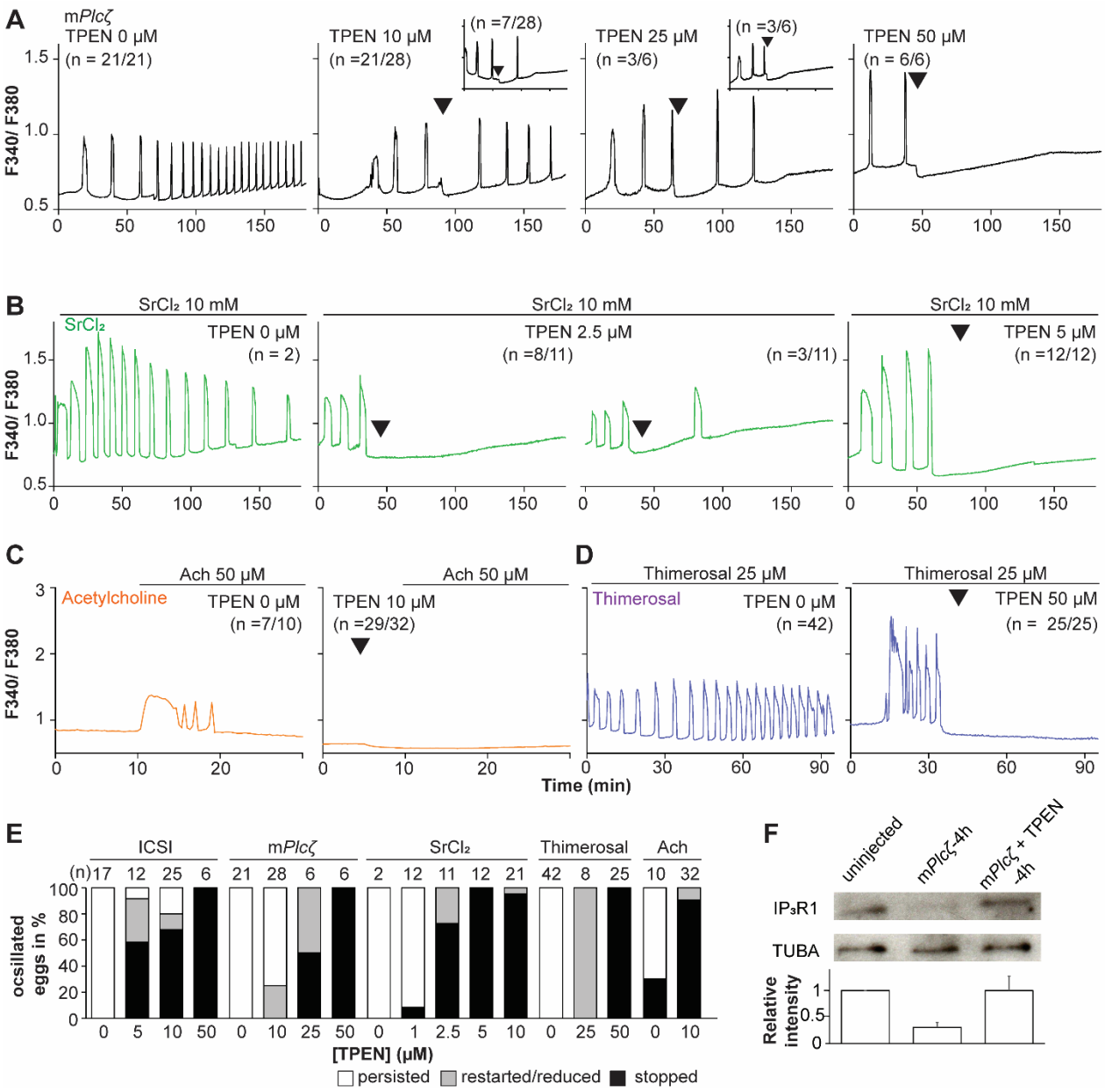

(**A-D**) Representative Ca^{2+} responses induced by (**A**) m*Plcζ* mRNA microinjection (0.01 μg/μl, black traces), (**B**) strontium chloride (10 mM, green), (**C**) acetylcholine chloride (50 μM, orange), and (**D**) thimerosal (25 μM, purple) in MII eggs. Increasing concentrations of TPEN were added to the monitoring media (arrowheads above traces denotes the time of adding). Insets in the upper row show representative traces of eggs that stop oscillating despite others continuing to oscillate. (**E**) Each bar graph summarizes the TPEN effect on Ca^{2+} oscillations at the selected concentrations for each of the agonists in A-D. (**F**) Western blot showing the intensities of IP_3R1 and alpha-tubulin bands in MII eggs or in eggs injected with m*Plcζ* mRNA and incubated or not with TPEN above ($P < 0.01$). Thirty eggs per lane in all cases. This experiment was repeated twice, and the mean relative intensity of each blot is shown in the bar graph below.

967 **Figure 3. TPEN inhibition of cIP$_3$-induced Ca^{2+} release is precluded by ZnSO$_4$ supplementation**
968 **before TPEN exposure.**

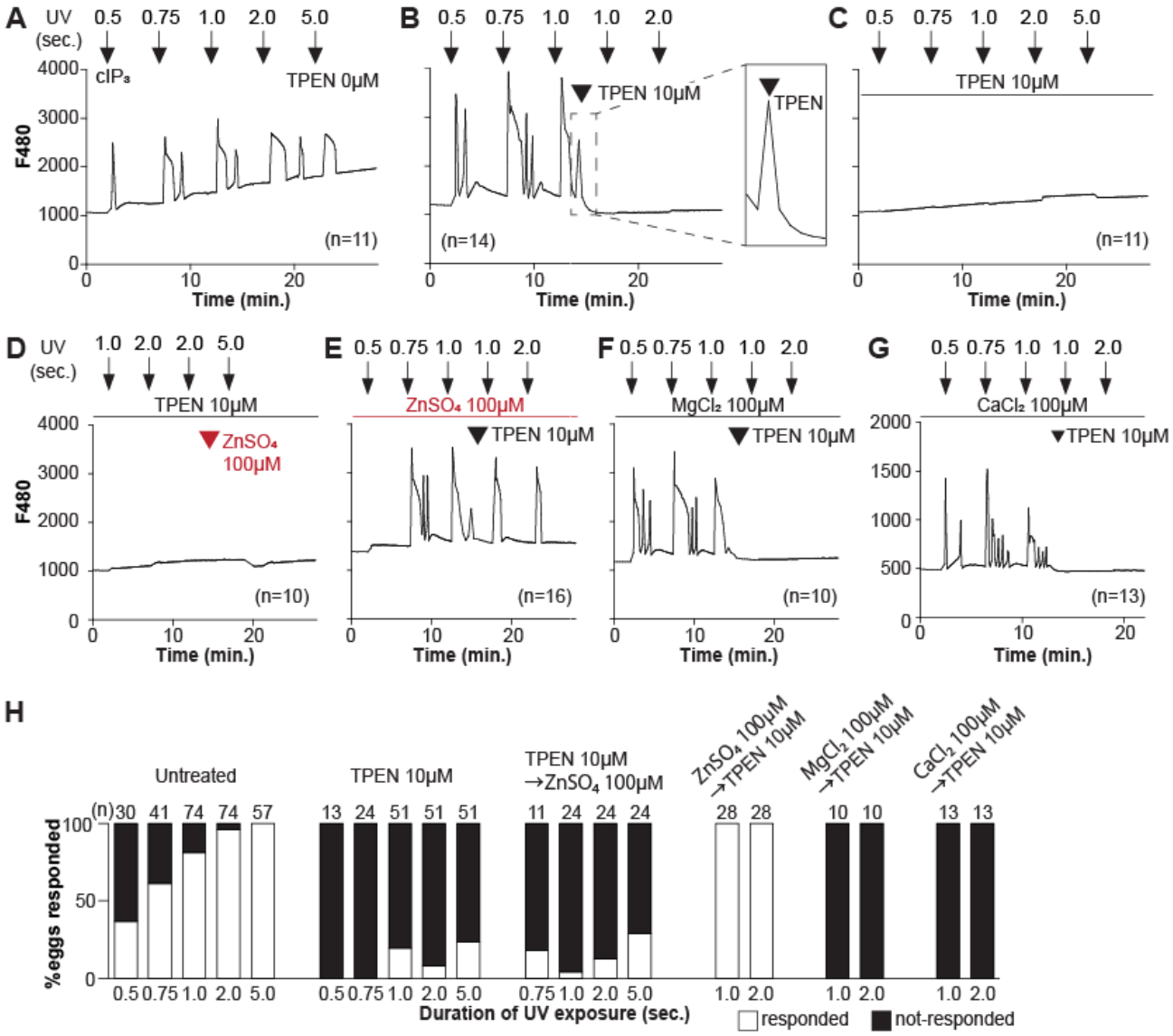

969
970 (**A-G**) Representative Ca^{2+} responses in MII eggs triggered by the release of caged IP$_3$ (cIP$_3$) induced
971 by UV light pulses of increasing duration (arrows). (**A**) A representative control trace without TPEN,
972 and (**B**) following the addition of 10 μM TPEN between the third and the fourth pulses. The broken
973 line rectangle is magnified in the inset, farthest right side of the panel displaying the near immediate
974 termination of an ongoing rise. (**C, D**) Recordings started in the presence of 10 μM TPEN but in (**D**)
975 100 μM ZnSO$_4$ was added between the second and the third pulses. (**E**) Recording started in the
976 presence of 100 μM ZnSO$_4$ followed by the addition of 10 μM TPEN between the third and the fourth
977 pulses. (**F, G**) Recording started in the presence of 100 μM MgSO$_4$ (**F**) or 100 μM CaCl$_2$ (**G**) and 10
978 μM TPEN added as above. Arrowheads above the different panels indicate the time of TPEN or
979 divalent cation addition. (**H**) Bar graphs summarizing the number and percentages of eggs that
980 responded to a given duration of UV pulses under each of the TPEN±divalent ions.

Figure 4. Zn^{2+} depletion alters Ca^{2+} homeostasis and increases Ca^{2+} store content independent of IP_3R1 mass.

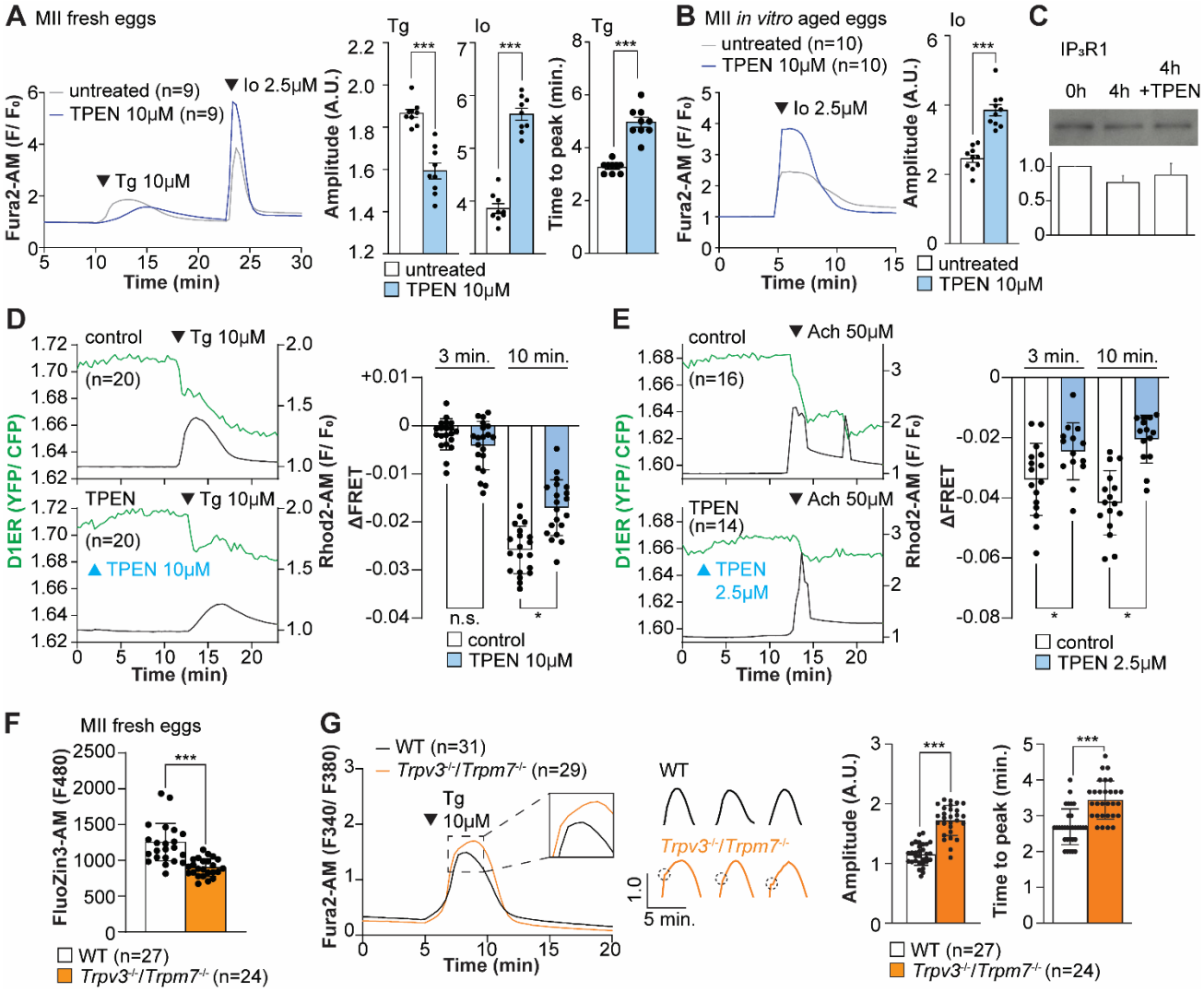

(**A, B**) Representative Ca^{2+} traces of MII eggs after the addition of Tg and Io in the presence or absence of TPEN. Blue trace recordings represent TPEN-treated eggs whereas gray traces represent control, untreated eggs. (**A**) Io was added to fresh MII eggs once Ca^{2+} returned to baseline after treatment with Tg. Comparisons of mean peak amplitudes after Tg and Io are shown in the bar graphs in the right panel ($P < 0.001$). (**B**) MII eggs were aged by 2-hr. incubation supplemented or not with TPEN followed by Io addition and Ca^{2+} monitoring ($P < 0.001$). (**C**) Western blot showing the intensities of IP_3R1 bands in MII eggs freshly collected, aged by 4-hr. incubation without TPEN, and with TPEN. Thirty eggs per lane in all cases. This experiment was repeated three times. (**D, E**) (Left panels) Representative traces of Ca^{2+} values in eggs loaded with the Ca^{2+}-sensitive dye Rhod-2 AM and the ER Ca^{2+}reporter, D1ER (1 μg/μl mRNA). TPEN was added into the media followed 10 min. later by (**D**) 10 μM Tg and (**E**) 50 μM Ach. (Right panel) Bars represent the difference of FRET value between at the time of Tg/ Ach addition and at 3 and 5 min. later of the addition ($P < 0.05$). Experiments were repeated two different times for each treatment. Black and green traces represent

997 cytosolic Ca^{2+} and Ca^{2+}-ER, respectively. Blue and black arrowheads indicate the time of addition of
998 TPEN and Tg/ Ach, respectively. (**F**) Basal Zn^{2+} level comparison in WT (open bar) and *Trpv3*$^{-/-}$
999 /*Trpm7*$^{-/-}$ (dKO, orange bar) MII eggs. Each plot represents the Fluozin3 measurement at 5 min. after
1000 starting monitoring. (**G**) (Left panel) Representative Ca^{2+} traces of WT (black trace) and dKO
1001 (orange trace) MII eggs after adding Tg. Insets represent the magnified traces at the peak of Ca^{2+}
1002 spike from different sets of eggs. (Middle panel) Individual traces of WT and dKO eggs after Tg
1003 addition. Dashed circles represent the flection point in dKO traces. (Right panel) Comparisons of
1004 mean peak amplitudes after Tg and the time between Tg addition and the Ca^{2+} peak are shown in the
1005 bar graphs in the right panel ($P < 0.001$)
1006

1007 **Figure 5. Restoring Zn^{2+} levels with ZnPT rescues oscillations interrupted by TPEN-induced**
1008 **Zn^{2+} deficiency.**

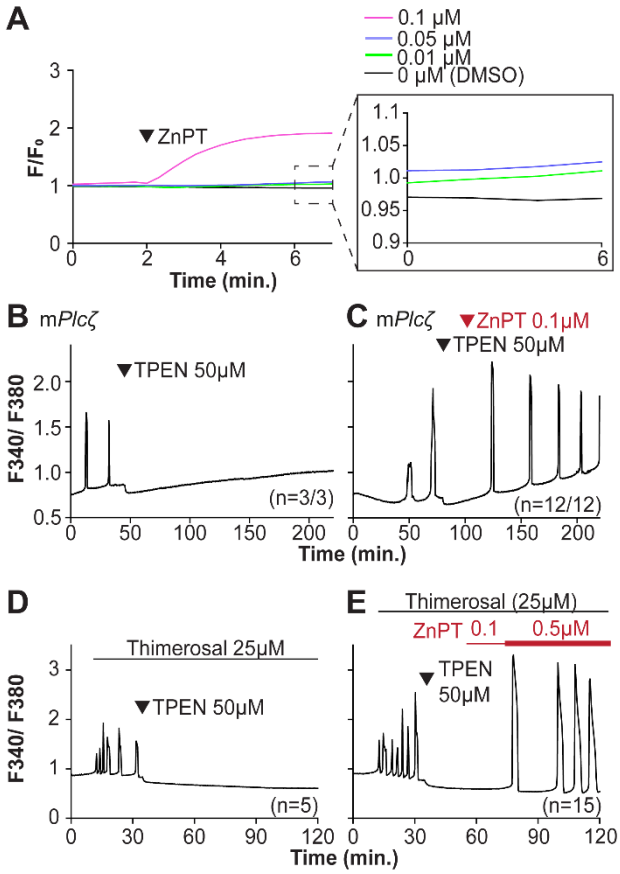

1009

1010 (**A**) Representative traces of Zn^{2+} in MII eggs following the addition of 0.01 to 0.1 μM concentrations
1011 of ZnTP. The broken rectangular area is amplified in the next panel to appreciate the subtle increase in
1012 basal Zn^{2+} caused by the addition of ZnTP. (**B, C**) m*Plcζ* mRNA (0.01 μg/μl)-induced oscillations
1013 followed by the addition of TPEN (black arrowhead) (**B**), or after the addition of TPEN followed by
1014 ZnPT (red arrowhead) (**C**). (**D, E**) Thimerosal (25 μM) induced oscillations using the same sequence
1015 of TPEN (**D**) and ZnPT (**E**), but higher concentrations of ZnPT were required to rescue Thimerosal-
1016 initiated oscillations (**E**). These experiments were repeated at least two different times.

1017 **Figure 6. Excess Zn^{2+} hinders Ca^{2+} oscillations.**

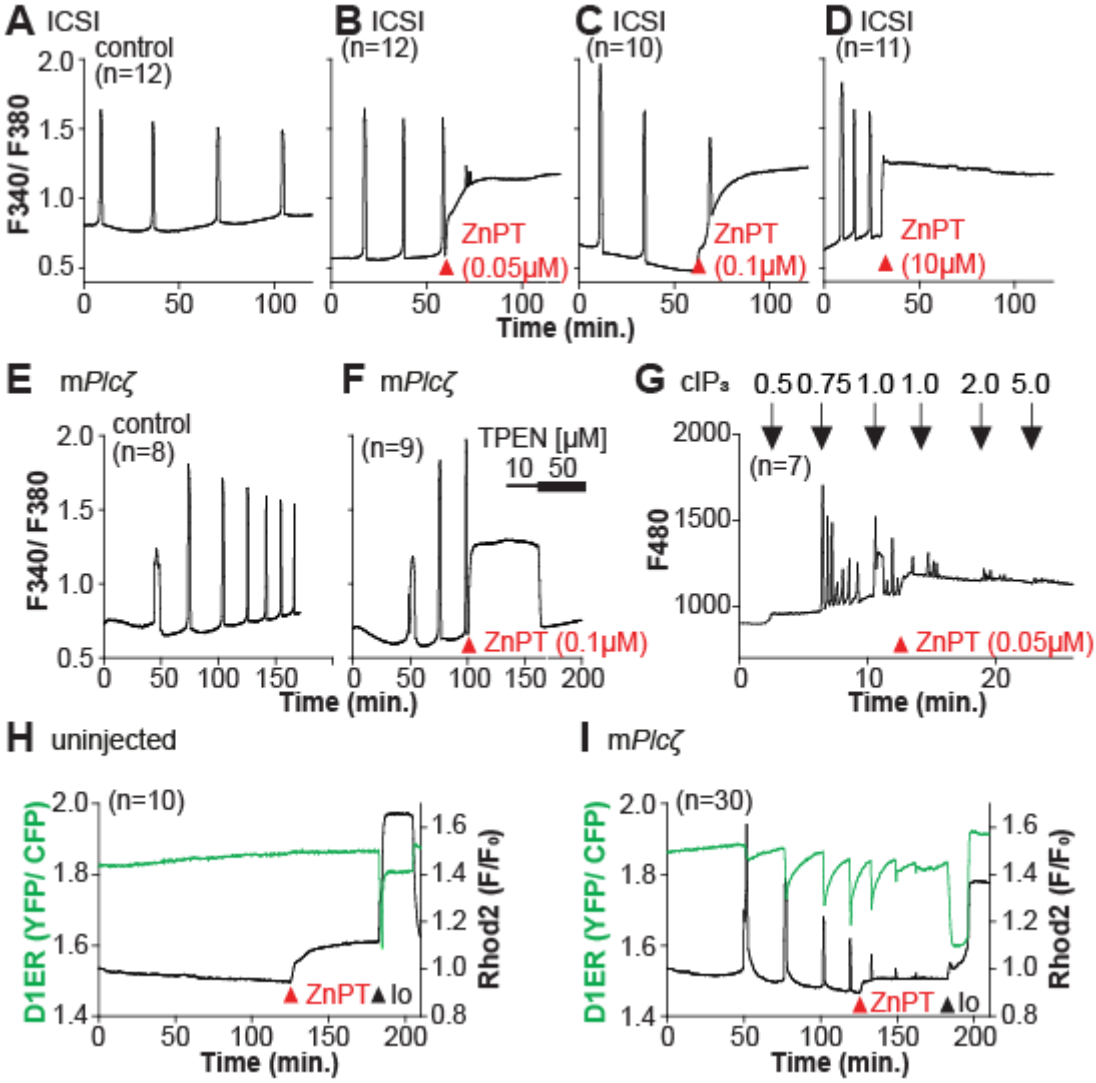

1018

1019 (**A-D**) ICSI-initiated Ca^{2+} response without (**A**) or following the addition of ZnPT (**B, C**) (the time of
1020 ZnPT addition and concentration are denoted above the tracing). (**E**, **F**) Representative Ca^{2+} responses
1021 induced by injection of 0.01 μg/μl m*Plcζ* mRNA in untreated eggs (**E**) or in eggs treated with 0.1 μM
1022 ZnPT followed by 10 μM TPEN first and then 50 μM (**F**). (**G**) cIP_3-induced Ca^{2+} release as expected
1023 when the UV pulses in the absence but not in the presence of 0.05 μM ZnPT (the time of addition is
1024 denoted by a bar above the tracing). (**H, I**) Representative traces of Ca^{2+} values in eggs loaded with the
1025 Ca^{2+}-sensitive dye Rhod-2 AM and the ER Ca^{2+}reporter, D1ER (1 μg/μl mRNA). Uninjected and 0.01
1026 μg/μl m*Plcζ* mRNA-injected eggs were monitored. After initiation and establishment of the
1027 oscillations, 0.1 μM ZnPT was added into the media followed 30 min later by 2.5 μM Io. Experiments
1028 were repeated two different times. Red and black arrowheads indicate the time of addition of ZnPT
1029 and Io, respectively.

Figure 7. Schematic of proposed regulation of IP_3R1 function by Zn^{2+} in eggs and fertilized zygotes.

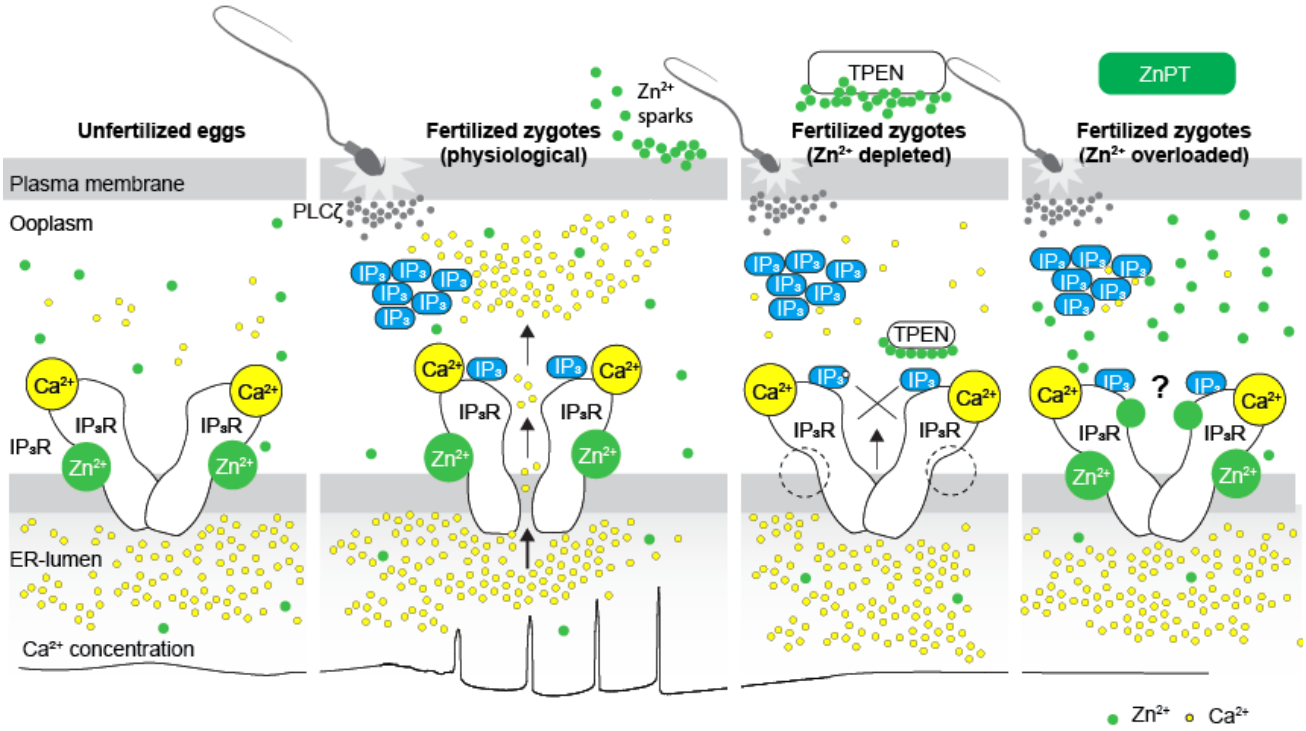

In MII eggs, left panel, IP_3R1s are in a Ca^{2+}-release permissive state with optimal levels of cytoplasmic Ca^{2+} and Zn^{2+} and maximum ER content, but Ca^{2+} is maintained at resting levels by the combined actions of pumps, ER Ca^{2+} leak, and reduced influx. Once fertilization takes place, left center panel, robust IP_3 production induced by the sperm-borne PLCζ leads to Ca^{2+} release through ligand-induced gating of IP_3R1. Continuous IP_3 production and refilling of the stores via Ca^{2+} influx ensure the persistence of the oscillations. Zn^{2+} release occurs in association with first few Ca^{2+} rises and cortical granule exocytosis, Zn^{2+} sparks, lowering Zn^{2+} levels but not sufficiently to inhibit IP_3R1 function. Zn^{2+} deficiency caused by TPEN or other permeable Zn^{2+} chelators, right center panel, dose-dependently impairs IP_3R1 function and limits Ca^{2+} release. We propose this is accomplished by stripping the Zn^{2+} bound to the residues of the zinc-finger motif in the LNK domain of IP_3R1 that prevents the allosteric modulation of the gating process induced by IP_3 or other agonists. We propose that excess Zn^{2+}, right panel, also inhibits IP_3R1-mediate Ca^{2+} release, possibly by non-specific binding of thiol groups present in cysteine residues throughout the receptor (denoted by ?). We submit that optimal Ca^{2+} oscillations in mouse eggs unfold in the presence of a permissive range of Zn^{2+}concentration.

Supplementary Figure 1. Overexpression of ER accessory protein ERp44 did not change the Ca^{2+} responses initiated by m*Plcζ* mRNA microinjection, Actylcholine, or $SrCl_2$.

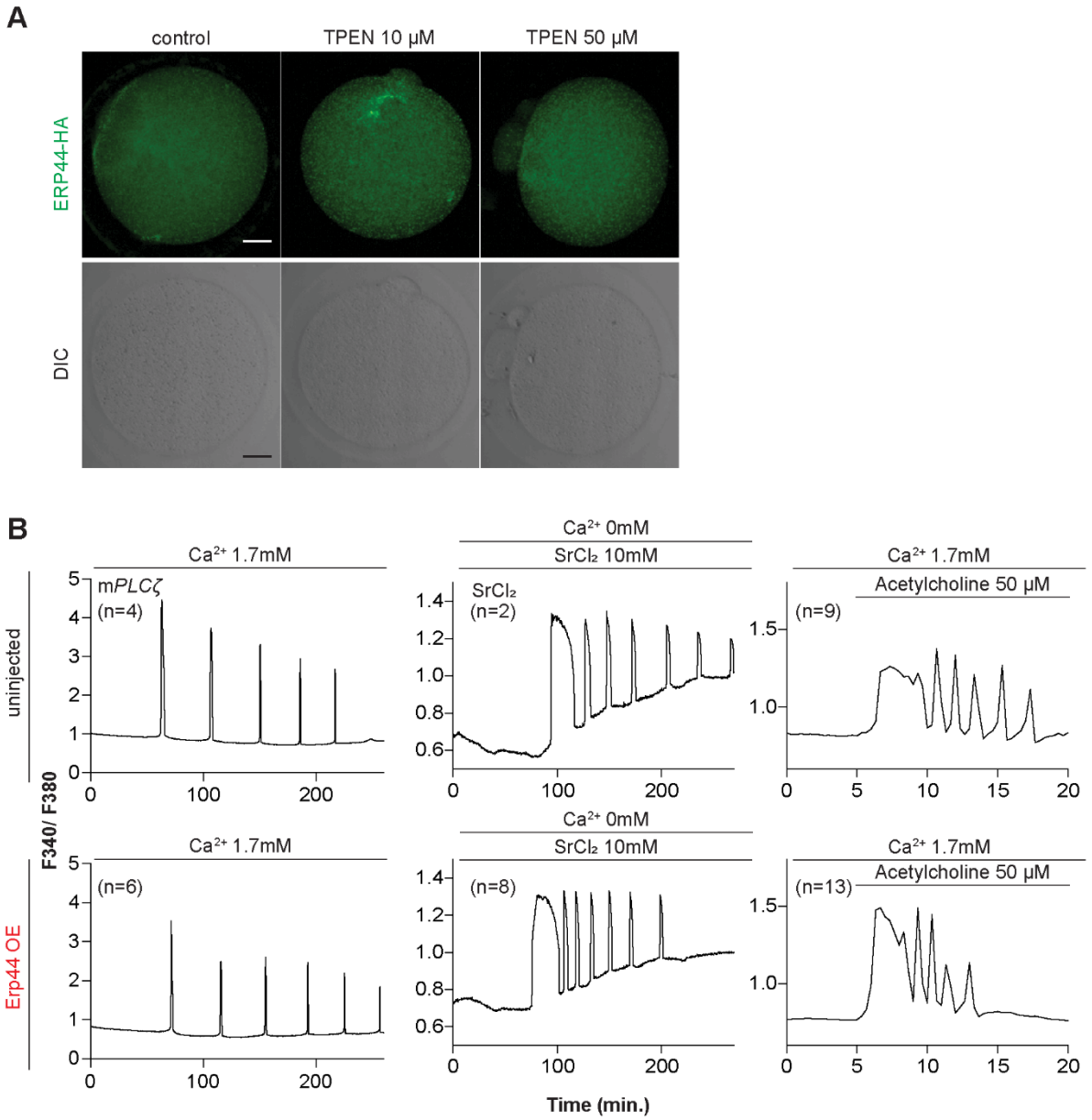

(**A**) Representative immunofluorescent images of MII eggs with overexpression of ERp44. At 5 hr. post microinjection, eggs were treated with 10 or 50 μM of TPEN and incubated for 1 hr, after which they were fixed and stained. An anti-HA antibody was used. Scale bar: 10 μm. (**B**) Representative Ca^{2+} responses induced by m*Plcζ* mRNA microinjection (0.01 μg/ μl-left column), $SrCl_2$ (10 mM-center column), and acetylcholine (50 μM-right column) in eggs with (top panels) or without (bottom panels) ERp44 overexpression.

Supplementary Figure 2. Elevated Zn^{2+} impairs egg activation and the subsequent embryo development.

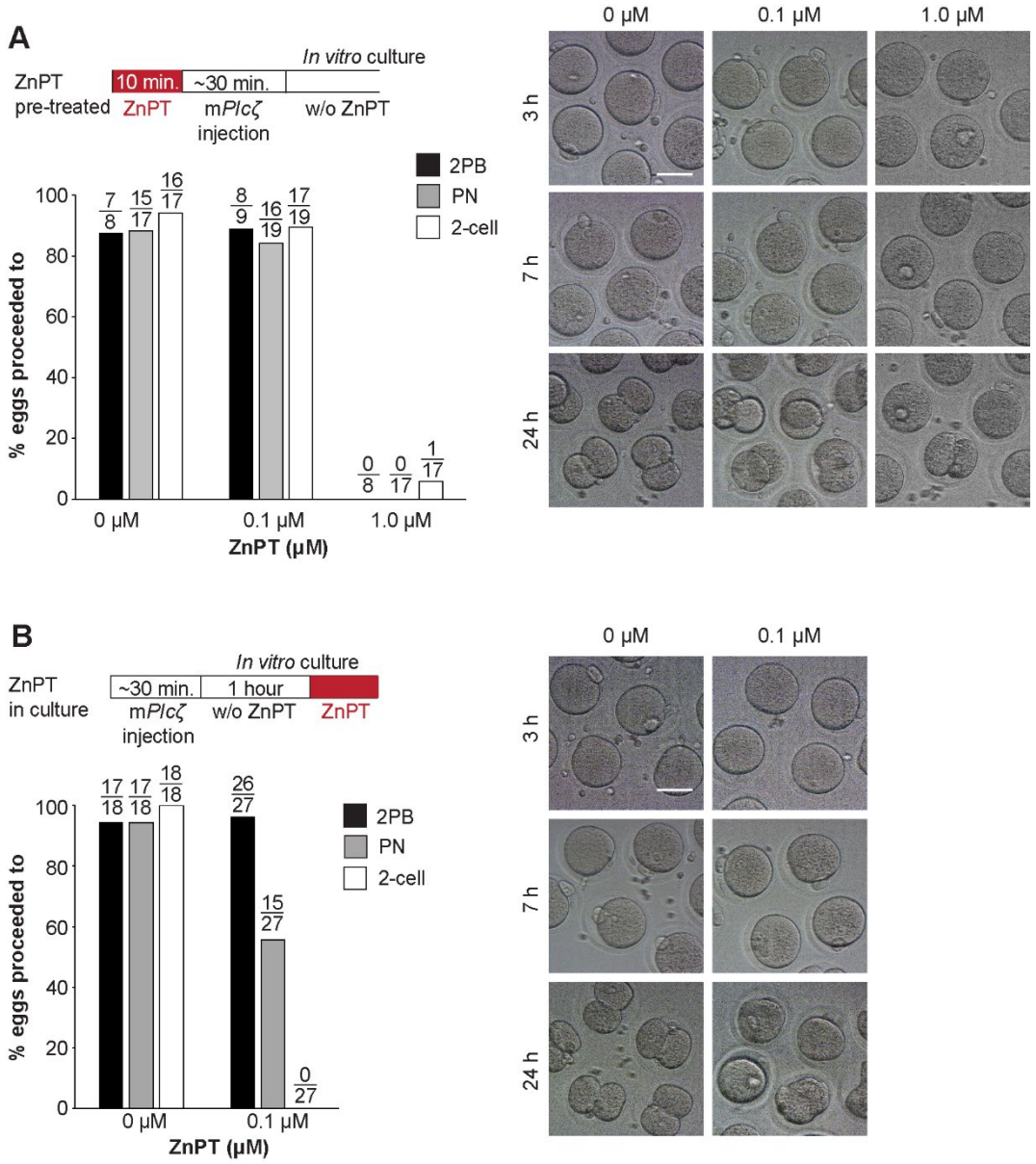

(**A**) MII eggs were incubated in TL-HEPES containing 0, 0.1, or 1.0 μM ZnPT at room temperature for 10 min and washed several times with fresh TL-HEPES and injected with m*Plcζ* mRNA. After it, eggs and zygotes were cultured in KSOM for 24 hr. PN formation and 2-cell development were checked at 7- and 24-hr post-microinjection. Bars represent the percentages of injected eggs that reached the PN and the 2-cell stage. Scale bar: 50 μm. (**B**) MII eggs injected with m*Plcζ* mRNA were incubated in KSOM without ZnPT for an hr. and then incubated in KSOM with 0 or 0.1 μM ZnPT for 24 hr. The second polar body extrusion, PN formation, and 2-cell development were checked at 2.5-, 7- and 24-hr. post-microinjection. Bars represent the percentages of injected eggs that reached the PN and the 2-cell stage. Scale bar: 50 μm.